MAPPING RIVERBED SEDIMENT SIZE FROM SENTINEL 2 SATELLITE DATA

Abstract

A comprehensive understanding of river dynamics requires the grain size distribution of bed sediments and its variation across different temporal and spatial scales. Several techniques are already available for grain size assessment based on field and remotely sensed data. However, the existing methods are only applicable on small spatial scales and on short time scales. Thus, the operational measurement of grain size distribution of river bed sediments at the catchment scale remains an open problem. A solution could be the use of satellite images as the main imaging platform. However, this would entail retrieving information at sub-pixel scales.

In this study, we propose a new approach to retrieve sub-pixel scale grain size class information from Copernicus Sentinel-2 imagery building upon a new image-based grain size mapping procedure. Three Italian gravel-bed rivers featuring different morphologies were selected for Unmanned Aerial Vehicle (UAV) acquisitions, field surveys and lab analysis meant to serve as ground truth grain size data, ranging from medium sand to coarse gravel. Grain size maps on the river bars were generated in each study site by exploiting image texture measurements, upscaled and co-registered with Sentinel-2 data resolution.

Relationships between the grain sizes measured and the reflectance values in Sentinel-2 imagery were analyzed by using a machine learning framework. Results show statistically significant predictive models (MAE of ±8.34 mm and R^2=0.92). The trained model was applied on 300 km of the Po River in Italy and allowed us to identify the gravel-sand transition occurring along this river length.

Therefore, the approach presented here - based on freely available satellite data calibrated by low-cost drone-derived imagery - represents a promising step towards an automated surface mean grain size mapping over long river length, easily repeated through time for monitoring purposes.

Keywords: Grain size mapping, Fluvial Remote Sensing, Sentinel-2, UAV, machine learning.

1. INTRODUCTION

A key variable to understand fluvial processes and to monitor river behavior is bed grain size distribution and its pattern of change along rivers over time. In fact, bed sediment size affects flow resistance, regulates channel morphodynamics, and influences fluvial ecosystems functioning. Linkages among bed sediment size, river morphology and ecological dynamics (Ferguson et al., 1996; Pitlick et al., 2008; Pizzuto, 1995; Rice, 1999; Rice and Church, 2001) call for grain size assessment carried out at large spatial scales, i.e., over most of the channel network (Dugdale et al., 2010). In fact, river systems and their biota respond and behave at large temporal and spatial scales (Fausch et al., 2002). However, the bulk of our scientific measurement and monitoring work occur at much smaller spatial scales which are usually further constrained by short temporal scales. These considerations are valid also for particle size measurement. Beside field-based surveys, remote sensing approaches to grain size mapping have been an active focus of research for over a decade allowing for the development of more objective and rapid methods (*e.g.* Black et al., 2014; Buscombe et al., 2010; Buscombe and Masselink, 2009; Carbonneau et al., 2018, 2004a, 2004b, 2005; Detert and Weitbrecht, 2012; Dugdale et al., 2010; Graham et al., 2005, 2010; Rubin, 2004; Verdú et al., 2005; Woodget et al., 2018).

Remote sensing approaches measure surface roughness, used as a surrogate for particle size estimation (Cavalli et al., 2008, Smith, 2014, Chappell and Heritage, 2007). This is due to different particles dimension, shape, spatial arrangement that generate a range of surface roughness, distinguishable from remote. Roughness detection and measurement depend on the specific wavelength used, i.e., a rough surface can appear smoother if shorter wavalengths are deployed.

The spectral properties of granular materials have been investigated mostly by soil scientists and civil engineers. Therefore, a direct application of their findings to fluvial sediments can require caution for the possible effect of particle transport and deposition. However, such studies relative to the spectral response of different soil types – which are summarized below – offer important insights on the factors which may potentially influence grain size estimation from satellite images.

An important finding is that the single scattering albedo of the smaller particles is greater than for bigger particles (Nash and Conel 1974, Pilorget et al., 2015, 2016). This has been demonstrated through laboratory experiments by Pilorget et al. (2013, 2015, 2016), who suggest that in the near-infrared region, even a small variation in the size of a mixture of particles with a given composition and scattering properties tends to control the overall photometric behavior. In Pilorget et al. (2016) the macroscopic roughness parameter, as defined by Hapke (1984), has been shown evolving with the wavelength and being to first order correlated with the absorptivity of the particles, thus mostly corresponding to a measurement of the particles shadowing. Additional support for this observation can be found in Carson et al. (2015), who finds from a physically robust modelling study that fine granular soils composed of quartzite and magnetite have a Bidirectional Reflectance Distribution Function (BRDF) intensity which is inversely proportional to wavelengths and therefore results in a systematically higher reflectance at longer infrared wavelengths for all view angles. Furthermore, Robinson and Friedman (2005) observed that the dielectric constant of materials composed of spherical particles can be affected by the geometry of the sphere packing arrangements. This finding is important because the reflectance intensity of an electromagnetic wave is proportional to the dielectric constant of the reflecting material (Marion and Heald, 1980), and thus, for longer wavelengths, the particle size of granular soils may affect the intensity of reflected radiation.

Remote sensing approaches for grain size mapping have been widely applied with high resolution imagery (mm-cm/pixels) where there is an implicit assumption that surface properties of sediment will affect image properties even if only using standard RGB imagery. Applications of this approach has led to a range of airborne and terrestrial remote sensing methods, each with well-documented errors, able to collect high resolution (mm to sub-mm) imagery suitable for the measurement of surficial particle size distribution (*e.g.* Detert and Weitbrecht, 2012; Graham et al., 2005; Rubin, 2004), and/or to generate mm-resolution topographic surveys by terrestrial laser scanning technology (Brasington et al., 2012; Heritage and Milan, 2009, Hodge et al., 2009) and/or SfM-photogrammetry point clouds useful to directly extract surficial grain sizes (Vázquez-Tarrío et al., 2017; Woodget et al., 2018).

A common approach used to derive particles size requires a measure of the surface texture derivable from the images collected by remote sensing techniques. Roughness can indeed be considered as a synonym of texture (e.g., Trevisani and Cavalli 2015, Cavalli et al., 2008; Grohmann et al., 2011). Within this approach, empirical correlation between some statistical properties of an image patch, such as co-occurrence textures or semivariance, and a measure of grain size such as median (D_{50}) or D_{84} values (e.g. Buscombe and Masselink, 2009; Carbonneau et al., 2004b, Chappell and Heritage., 2007) has to be established.

4

Unmanned Aerial Vehicles (UAVs, also referred to as drones) has been one of the most used and promising technology for several river surveys practices in the last decades. However, although the current UAV technical properties would permit low-cost measurement of several river attributes over kilometric scales, this technology cannot extend river surveys up to large catchment, regional or continental scales, and acquisitions at high temporal frequencies are difficult.

In contrast, little investigation has focused so far on the sub-pixel (10^{-2} to 10^{0} m/pixel) imagery for grain size mapping. Black et al. (2014) attempted to use hyperspectral data from aircraft technology (image resolution of 3 cm/pixel). Their results suggest that sandy patches reflect more brightly than larger particles in the red and infrared region. Satellite data, despite their low spatial resolution (m/pixel), have been used in sub-pixel methods to study landscape units with characteristic dimensions below 100 m or even below 10 m (Busetto et al., 2008; Verhoeye and De Wulf, 2002). A recent study by Purinton and Bookhagen (2020) showed that radar amplitude collected by several satellites, with different wavelength and resolution, have the potential to identify sediment size in mixed sand- and gravel-bed rivers.

In this work, we aim to investigate the potential of retrieving sub-pixel scale grain size information from Copernicus Sentinel-2 imagery. The approach combines low-cost UAV imagery to calibrate robust linear correlations between grain sizes of dry exposed river bars and reflectance values from Sentinel-2 imagery. We hypothesize that: (i) there is an inverse correlation between grain size and Sentinel-2 reflectance data; (ii) such a correlation, calibrated by UAV imagery and field data, permits to infer mean grain size of exposed sediment bars by means of Sentinel-2 reflectance data; (iii) the gravel-sand transition in the Po River (Italy) can be detected by Sentinel-2 reflectance data.

5

2. METHODS

2.1 Study areas

Six study sites, correspondent to exposed sediment bars, were selected along three Italian gravel-bed rivers: Po, Sesia and Bonamico (Figure 1). The choice of these sites was driven by the need of having a heterogeneous dataset in terms of grain size and lithology and large (>100 m^2, to account for the Sentinel-2 pixel size 10mx10m), homogeneous and unvegetated sediment bars. The prerequisites of a wide range of climatic and lithologic conditions, met in the geographic variety of reaches selected, was intentional: having various lithologies and environmental conditions allow to highlight and focus on the correlation between roughness and D_{50}. Four study sites lie in Northern Italy: three on the Po River and one on the Sesia River. The Po River is the largest Italian river, both in terms of length (652 km) and drainage basin area (about 74,000 km^2). The wide alluvial plain of Po River is almost unique for its large variety of lithological and structural features. It is developed within a highly variable geomorphological framework, correspondent to a complex geologic and tectonic context. Throughout its length the Po River receives contributes from both Alpine and Appennine tributaries, that carry sediments of different lithological origin. The geological units range from deep lithospheric mantle rocks to oceanic basalts and relevant sedimentary covers, from the plutonic and volcanic continental rocks to the overlying carbonate and siliciclastic sedimentary covers, as well as to many kinds of metamorphic rocks (source: official webgis ARPA Piemonte). Within the channel these sediments are all recognized under the category of fluvial deposits. The Po valley is one of the most populated and productive areas of Italy, so that human activities have deeply modified the Po River behavior over the centuries (Gumiero et al., 2009, Marchetti 2002, Surian and Rinaldi 2003). Along its length, the Po River displays a wide spectrum of channel patterns as consequence of both natural and anthropic factors, including single-thread sinuous and meandering, transitional and multi-thread braiding patterns. River bars are mostly dominated by gravel down to the confluence with the Ticino River. Downstream of this section, the Po channel becomes narrower with a sinuous to meandering pattern, and displays alternate and point bars mainly composed of sand. The three study sites along the Po River are located upstream (site P1, Fig. 1) and downstream of the Ticino confluence (sites P2 and P3, Fig. 1).

The Sesia River (basin area of around 2920 km^2) is an important Alpine tributary of the Po River, which feeds the latter with high volumes of bedload, ranging in size from coarse

6

gravels to cobbles. Morphologically, once the Sesia leaves the confined reaches within the Alps, it features island-braiding channel pattern, which downstream evolves into a single thread meandering channel. As regards lithology, the river starts in a confined channel in the Alps characterized by metamorphic units (Gneiss, Schist, Acid igneous rock, Marble, Orthogneiss, Granulite, Paragneiss). Moving downstream to the valley sedimentary rocks (conglomerate, terraced alluvial and debris flow deposits) are predominant (source: official webgis ARPA Piemonte). The study site on the Sesia River is located in the Piedmont part, along the island-braiding reach (site S1, Fig.1), characterized by a gravel bed, close to the town of Arborio.

Finally, the last two study sites (B1 and B2 in Fig.1) were selected in the Calabria Region (Southern Italy) along the Bonamico River, a short length watercourse (18 km) draining a small-sized catchment (about 136 km^2) starting from the Aspromonte Massif and flowing in a very steep valley. This typical watercourse, called '*fiumara*', features a large supply of coarse sediments (gravel and cobbles) and an active braiding pattern. The lithology of the area is predominantly composed by metamorphic Variscan complex terrains (Carbonifero-Permiano) and fragmentary sedimentary cover (from Mesozoic to Pleistocene) composed of: conglomerates in arenitic matrix, of metamorphic or granitic nature, late-orogenic flysch deposits (Oligocene superior – Miocene inferior) and antisicilidi clays which close the sequence of the nappe-pile tectonic stack (The youngest sedimentary deposits are the Lower Pleistocene marine terraces) (source: geological map of Italy, ISPRA 2011).

Figure 2 reports the methodological workflow embraced by this study and includes a i) ground-truthing step of grain size analysis on the study sites; ii) a satellite-based analysis on the same study sites, and iii) an application of the grain size prediction model derived from steps i) and ii) to sediment bars selected along 300 km of channel length in the Po River from the city of Torino (Piedmont Region) to the town of Casalmaggiore (Lombardy Region). These steps are illustrated in detail in the following sections. The overall framework was conducted in QGIS and Python.

2.2 Ground truthing data acquisition and analysis

Ground-truthing data for sediment size distribution on river bars were collected at different times and with different techniques, exploiting both high resolution drone imagery and field

7

sampling with subsequent lab sieving. Two different procedures were then applied to grain size data measurement to obtain a grain size map on the entire sediment bars, used as training data for machine learning models.

Drone flights were conducted on the 20th and 21st September 2018 in the Po and Sesia rivers respectively (sites P1 and S1; Fig. 1), and in the 23rd and 24th October 2018 in the Bonamico River (sites B1 and B2; Fig. 1). Dates of flight were characterized by sunny and dry conditions. Surveys were conducted by a DJI Phantom 4 Pro drone for images acquisition and by a Trimble R10 RTK-GPS for ground target data collection at cm-accuracy (the number of ground control points per site are 18 for P1, 13 for S1, 11 for B1, 13 for B2). The UAV images were acquired at 80% forward overlap and 50% sidelap, at different altitudes: one flight at around 50 m above ground level to collect RGB imagery of the whole site, whereas other flights were conducted at 20 m and further near ground at 5-7 m. Low altitude images were collected to cover the whole grain size range found on river bars and later used to extract the ground truth grain size data). Flight patterns for the acquisition of photosieving imagery were based on Carbonneau et al (2018). This method also delivers optimal results for terrain mapping by using established flight patterns that involve oblique imagery and acquisition at multiple altitudes.

Agisoft Metashape software Professional Edition, version 1.6, was used to process all UAV images (50, 20 and 5-7 m altitude) and to produce orthophotos with a spatial resolution of 2 cm. In the orthophoto process generation the blending mode and hole fitting mode were unchecked to minimize blurring and/or distortion effects. The near ground images at 5-7 m above surface were used to detect particles down to a size of about 3 mm, over an area of around 100 m^2 per image. From each image, an automated photosieving process, using PebbleCounts software (Purinton and Bookhagen, 2019), was used to determine surface grain sizes and sand percentage. The photosieving technique is a well-established methodology used to measure superficial grain size distribution from high resolution images. This technique finds some limitations when there are blurred patches and/or distortions within the image so that a carefully choice of suitable images was made. Another limitation of this technique is linked to the presence of irregular shape, not well recognized by the software, that reduce the performance of the technique. In our case, most of the grains in all sites were characterized by rounded shape, typical of fluvial deposits. For these considerations, we can assume that results obtained by the photosieving technique is comparable with those reported in literature. Carbonneau et al

8

(2018) and Dugdale et al (2010) have summarized our current knowledge on the errors associated to photosieving methodologies. The consensus view is that these are constrained in the area of 0.05ψ to 0.33ψ.

Diameter percentiles considered were the D_{50} and D_{84}. The large particle-size fractions are indeed those that influence most the surface roughness and can be exploited for the purpose of this study. The presence of fine particles in the interstitial area between gravels affects image texture thus it needs to be accounted for. To include the sand percentage data (% sand), the final D50 percentile value was calculated as $D_{50} \times (1 - \% sand)$. The same procedure was followed for the D84 percentile. A total of 48 particle percentiles values (for D50 and D84) were measured in all sites.

To enlarge the dataset, a texture-based grain size mapping approach was used to derive grain size measurement from the UAV orthoimage texture. The idea behind is to use cm-scale resolution UAV orthophotos to generate grain size maps of the entire sediment bars under study. Texture-based grain size mapping approaches are well established in literature (Woodget et al 2018, Carbonneau and Lane 2005) showing strong linear relationship between surface grain size and the texture properties of remotely sensed data. The next steps of the analysis were conducted in Python with emphasis on the scikit-learn and scikit-image libraries (Pedregosa et al., 2011; Walt et al., 2014) which offer high-level routines for machine learning and image processing, including texture calculation. A range of 33, 51 and 101 kernel window sizes were used, based on previous experience (Carbonneau 2005, Black et al., 2014) to calibrate the surface grain size determination models. The window for the Gray Level Co-occurrence Matrix (GLCM) calculation, needed for dissimilarity algorithm application, was centered at the XY location of the ground truth data collected by the photosieving technique. A linear model was used to fit the dissimilarity extracted values and the D_{50} diameter with a 5-fold cross validation, later used to generate the grain size map of each sediment bar. As noted by Woodget et al. (2018), often the SfM orthorectification process limits the strength of the results obtained with texture-grain size approach. To avoid the inclusion of blurred patches and limit the disturbance linked to different light conditions between different lines of flight, the texture-grain size approach was limited to tiles of 8x8 m cut on the orthophoto centered on the XY cameras positions. After a manual selection of tiles not contaminated by water and vegetation, dissimilarity values were extracted for each tile, with a moving window of 101x101 pixels (in orthophotos with a pixel size of 2 cm). The texture-grain size model previously calibrated was thus used in prediction and the median diameter value calculated in each 8x8 m tile was taken as reference grain size percentile for the correspondent XY sampling location. Moving to QGIS, the dataset was interpolated exploiting the GRASS v.bspline command, to generate a grain size map for each site with the same resolution (10 m/pixel) and coordinate system of Sentinel 2 data. Resulting grain size maps were readily comparable with reflectance values of Sentinel 2 images since they overlap perfectly with the corresponding Sentinel 2 pixels.

In addition to UAV-based ground-truthing on gravel bars, in April 2021 field samplings in the Po River were carried out to enlarge the dataset to the sand-dominated bars (sites P2 and P3, Fig. 1). For such sediment size, the application of the photosieving technique is not feasible, and laboratory analysis were necessary on sediment samples. Two sand bars downstream the confluence with the Ticino River (sites P2 and P3; Fig. 1) were sampled, characterized by homogeneous grain size distribution through the entire bar. A total weight of 2.4 kg for site P2 and 3.6 kg for site P3 were sieved to measure particles dimensions. Sampling sediments, carried out in the first 10 cm of the soil bars, did not show stratification in the upper layer. A grain size map at 10 m resolution was generated for each bar by assigning the median diameter derived from the two field samples, by assuming a uniform superficial grain size distribution, as assessed in the field.

2.3 Sentinel 2 data extraction

Sentinel 2 multispectral data were downloaded from the Copernicus services data hub (https://scihub.copernicus.eu/) for each selected site. Acquisition time was selected as the closest to the field work date, avoiding cloudy days with no visibility. Additional checks were also performed to ensure no rainfall occurred in the 3 days prior to Sentinel image acquisitions. Furthermore, discharge values from the nearest upstream gauging station and precipitation records were checked to control hydraulic conditions. Indeed, wet soils have a much higher dielectric constant and so appear much darker (Swain and Davis 1978). This means that the approach tested here should be restricted to dry sediment bars. Following these prerequisites Sentinel 2 data were downloaded at level 2A products (with full atmospheric correction) on the 24th of September 2018 for the tiles TMQ and TNQ, covering Sesia and Po rivers (sites S1, P1, P2, P3, Figure 1); on the 22nd of October 2018 for the tile SWC covering the Bonamico river (sites B1 and B2, Figure 1). The output products of the atmospheric correction step are: four bands at 10 m: 490 nm (B2), 560 nm

10

(B3), 665 nm (B4), 842 nm (B8); nine bands at 20 m: 490 nm (B2), 560 nm (B3), 665 nm (B4), 705 nm (B5), 740 nm (B6), 783 nm (B7), 865 nm (B8a), 1 610 nm (B11), 2 190 nm (B12); three bands at 60 m: 443 nm (B1), 945 nm (B9) and 1 375 nm (B10). The Super resolution algorithm available as the Sen2Res plugin for the ESA SNAP open-source software, was used to super resolve the available bands at 10 m resolution (Brodu et al., 2017). In this work bands 1, 9 and 10 were not used because were designed to detect atmospheric quantities, thus the 10 bands available from VIS to SWIR region constituted the reflectance dataset. The super-resolution method has a high computational cost but it was necessary in this work, in accordance with the requirement needed by the Fuzzy logic classifier of Carbonneau et al., 2020.

Fuzzy classification of the Sentinel-2 imagery was used to select field samples generated from the UAV work described above. Our initial UAV grain size maps could include sediment patches that have a small percentage of water or vegetation which is well below the size of a single Sentinel-2 pixel. Given that these 2 components interact strongly with infrared radiation, their presence at a sub-Sentinel-2 pixel scale can substantially degrade the quality of a grain-size mapping process based also on infrared reflection. The last step of the procedure was therefore to filter and select only pixels belonging to dry sediments clear of vegetation. The fuzzy classifier developed in Carbonneau et al., 2020 infers sub-pixel composition with median errors ranging from -0.05 to 0.02 and mean absolute errors ranging from 0.14 to 0.21 and predicts the membership percentage of three classes of pixels: water, sediment and vegetation. This allowed for the selection of a total of 4597 sediment pixels, later available to train the model, of which 2404 belong to the sand class (amount of pixels on the sand bars P2 and P3) and 2193 belong to the gravel sediment class (amount of pixels on the gravel dominated bars S1, P1, B1, B2).

2.4 Models training and assessment

The dataset for the development of the grain size mapping model is composed of 4597 grain size values (D_{50} percentile, see section 3.1 for the explanation of why we used the D_{50} only) and 4597 corresponding radiance values registered from Sentinel 2 in 10 bands, which correspond to 4597*10 m^2 of exposed, unvegetated sediment bars (Fig 1).

First, the spectral signature of each study site and that of each sediment class was analyzed to investigate the potential of the dataset collected and to test the hypothesis of an inverse correlation between grain size and reflectance data of Sentinel 2. As already

11

mentioned above, the spectral signature of soils follows a common pattern along the electromagnetic spectrum, differing based on several parameters, such as surface roughness. To build the spectral signatures of each sediment bar, the average of the reflectance data was calculated and plotted against the wavelengths. The same plot was done by splitting the dataset in four grain size classes, from medium sand to coarse gravel, and averaging the radiance values of each class, in each wavelength available.
Second, supervised machine learning techniques were used for model training in Python. Response variables are the 4597 grain size values, and predictor variables are the 10 bands corresponding reflectance values. Regression models were trained, both linear (Huber regression) and nonlinear (Random Forest, DNN). The Mean Error (ME) and Mean Average Error (MAE) were applied to a 20% portion of the dataset set aside and not used in model training. The resulting error metrics are used as performance metrics to select the most meaningful model. Alternative model configurations were tested by selecting the most meaningful bands as candidate predictors for the observed diameter percentile (D_{50}). Furthermore, logistic regression was used as a binary classification algorithm to distinguish sand and gravel. The threshold was set at 2 mm, 22.6 and 32 mm, to discriminate between fine (sand) and coarse (gravel) particles in the dataset, following the Wentworth scale (Wentworth, 1922). Model assessment was evaluated looking at the confusion matrix scores (https://scikit-learn.org/stable/modules/generated/sklearn.metrics.confusion_matrix.html), used to summarize the prediction made by the binary classification model. The binary classifier calibrated can make two types of errors: it can incorrectly assign a class who defaults to the no default category, or it can incorrectly assign a class who does not default to the default category. Thus, the confusion matrix shows which of these two types of errors are being made.

2.5 Model prediction

The regression model derived as explained above was applied to predict grain size of exposed sediment bars selected along 300 km of the Po River (Figure 1). The aim was to test the model for large scale surface grain size mapping and to validate the model in terms of transition from gravel to sand dominated bars. The same procedure described in 2.2, based on the Fuzzy logic classifier of Carbonneau et al. (2020), was applied on the Po River corridor to select Sentinel-2 pixels corresponding to sediment bars. Figure 3 reports an example of two river reaches, selected in a wandering reach and in a sinuous reach classified into three fuzzy members: water, sediment and vegetation. Each pixel was assigned to each class with a probability (value from 0 to 100%), resulting from the fuzzy logic approach. Only pixels classified with a score > 95% were used in this work for the model prediction.

To visualize the longitudinal grain size variation predicted, a distance value was assigned to each pixel identified as sediment. A vector line following the river channel was delineated in QGIS and its vertexes were stepped up and extracted. The cumulative distance value was automatically calculated for each vertex, together with its projected coordinates (mgrs grid zone: UTM 32T). The resulting output was a raster where each sediment-classified pixel has been assigned both longitudinal distance and a D_{50} value. The model was applied using the reflectance values of Sentinel 2 data, collected on the 14th of September 2020. This date was selected following the criteria of no rain events in the previous three days, in a season coherent with the field data acquisition of the gravel bars, in a year (2020) in between 2018 and 2021, when field activities were carried out. Moreover, some field activities were carried out to check and validate values predicted on the sand dominated bars.

3. RESULTS

3.1 Texture-based model for grain size estimation from UAV images

Table 1 reports the ground truth data (D_{50} and D_{84} values), obtained as the value of the total samples collected per site and the area covered in each site. As it can be noticed, the grain size range goes from sand to gravel class. The median diameter of the site P1 in the Po River - about 100 km upstream from the city of Torino - is 35 mm and the D_{84} is 49 mm. The median diameter of the Po River sites P2 and P3 – located downstream close to the city of Cremona - ranges from 0.43 to 0.35 mm (D_{84} from 0.8 to 0.6 mm). These bars are mostly composed of sand, with occasional patches of finer sediments. The site S1, selected along the Sesia River near the town of Arborio, is characterized by a coarse sediment bar with a cobble bed (D_{50} = 42 mm, D_{84}=88 mm). Along the Bonamico, sites B1 and B2 feature a D_{50} of 33 mm and of 42 mm, and a D_{84} of 71 and 69 mm, respectively.

In Figure 4a the 48 D_{50} values extracted by UAV-based photosieving on all study gravel bars are plotted against the corresponding texture dissimilarity values (see section 2.2). A linear relationship between median diameters and the texture metric is apparent.

As expected, as the median diameter increases the texture of the image window, and hence the difference in brightness between adjacent pixels, increases. A linear model was used to fit the data, with a 5-fold cross validation. Figure 4b shows the observed vs predicted values, and a R^2 = 0.78 is obtained. The Mean Absolute Error (MAE) resulting from the 5-fold cross validation results to be 5.5 mm with a standard deviation of ±0.23 mm. This model was used to predict grain size data on the entire river bars and generate a grain size map (of D_{50}) at 10 m resolution (Sentinel 2 resolution), thus increasing the sampling dataset from 48 up to 4597 values. The same model calibration procedure was carried out for the D_{84}, values, obtaining a R^2 = 0.66, MAE = 4.3 mm with a standard deviation of ± 1.1 mm. Considering such results, all the subsequent analysis presented in this paper have focused on the D_{50} only, for sake of conciseness.

3.2 Spectral signatures from Sentinel-2 images

Figure 5 shows the analysis made on the 4597 grain size values (D_{50} values) and the corresponding Sentinel 2 radiance values super resolved at 10 m resolution, made to investigate the potential of the dataset collected and to test the hypothesis of an inverse correlation between grain size and reflectance data of Sentinel 2.

In Figure 5a the average of the reflectance value of each sediment bar is plotted versus each wavelength of Sentinel 2. Overall, as expected, the spectral signatures follow similar trends at all sites (Swain and Davis 1978). Sand-dominated sites (P2 and P3, Fig. 1) with a D_{50} of about 0.5 mm, have the highest reflectance over the whole spectrum. As grain size increases (D_{50} in the range of 25-40 mm) the overall spectral signature has lower values. Gravel bars in the Sesia and Po rivers (sites S1 and P1) feature a median diameter of 30-40 mm, and plot very close to the sand sites in the VIS region but are well distinguishable in the NIR and SWIR region. Gravel bars in the Bonamico River (sites B1 and B2) feature D_{50} values in the range 30-40 mm – i.e. very similar to the Po and Sesia gravel bars - but differ considerably in terms of spectral signature.

Figure 5b illustrates the clear effect of grain size on the spectral signature. In fact, it is evident how fine to coarse sand grain sizes feature higher reflectance in the whole spectrum compared to gravel grain sizes. At larger wavelength (beyond 950 nm) more sediment classes can be differentiated. Overall, Figure 5 confirms the hypothesis of an inverse correlation between surface grain size and reflectance data.

3.3 Calibration of the grain size predictive model from Sentinel 2 multispectral data

Multiple linear (Huber regression) and nonlinear (Random Forest, DNN) regression models were trained, where response variables are the 4597 D_{50} values and predictor variables are the 10 bands corresponding Sentinel 2 reflectance values. Table 2 reports the performance metrics resulting from the calibrated models.

The test set is used to assess the models. All models perform reasonably well, revealing robustness in the fitting and suitability of the dataset. The coefficient of determination R^2 is quite high in any model, ranging from 0.92 to 0.98 for Random Forest. The absence of large errors can be noticed, and the Mean Absolute Error (MAE) and the Mean Squared Error (MSE) remain stable between the test data and the training data.

The Huber regressor was chosen to be the most appropriate for the purpose of this study because: model performance in calibration, stability, absence of outliers, insights into the physical explanation behind the observed phenomena, model performance in application, and computational time. The Random Forest model was abandoned because of overfitting issues linked to the strong non-linearity of the model and its tendency to learn the noise in data rather than an overall trend. Figure 6 shows the good performance of the Huber regression model, resulting in predicted values close to the observed data values. Results show a suitable predictive performance, which is similar for all the sites thus indicating that the model is consistent and robust.

The Huber regression model performs within ± 2.85 mm. To this value it needs to be added the error of which the grain size dataset is affected, as derived from the texture-based model (MAE for D_{50} is 5.51 mm, see section 3.1). Thus, the overall prediction error is ±8.36 mm. Nonetheless, a gap in the dataset is present in the grain size range 1-10 mm, as investigated bars were either finer or coarser than these sizes. Looking at the sand class data some sand particles diameters are assigned with a negative value. This has no physical meaning but is explained by the total error of about 10 mm of the model and by the linear model functioning. A linear regression learns a model which is a linear combination of features of the input examples. In table 3 the coefficients of each band in the linear combination are reported.

Among all the wavelengths analyzed, the SWIR band B12 has the highest (negative) coefficient, which reveals the significance of this band in the model and the inverse correlation with the grain size. The B8 band in the NIR region seems also quite important, still with a negative relation with sediment size. All other bands appear to contribute to the regression with different signs. However, it is noteworthy that if we look at the results of single linear regression model (i.e., each Sentinel 2 band used as single and unique input for the classification model), each single band show a negative coefficient (Table 4).

In Table 4, values relative to R^2 and to the coefficients of the regression and the correlations between grain sizes and each band reflectance values are reported. This analysis shows that for all bands there is a certain degree of inverse correlation with the median diameter, confirming the most important physical effect behind the observed trend. Moreover, it shows that the most meaningful bands (R^2 values above 0.4) are in the SWIR region, coherently with the results obtained with the model using all bands as input (see Table 2 and 3). More parsimonious model calibrations with two or three bands as input were also attempted (data not shown). The 10 bands model was used in this study, because it achieves the best model performance compared to model with selected bands and because we did not see any specific reason to remove one band compared to another.

Logistic regression models were also trained on the 80% of the dataset to discriminate between fine (sand) and coarse (gravel) patches. In Table 5 the confusion matrix - resulting from the test set composed of 920 grain size values - is reported, , which summarizes the performance of the binary classification model (based on 2 mm, 22.6 and 32 mm as thresholds).

16

The confusion matrix shows that of the 434 data > 2 mm the model classified 86 of them as lower than this threshold, and thus 348 are true positives (TP) and 86 are false negative. With regards to the finer class, the total number of data were correctly classified (TP = 486). Model performance assessment shows that 2 mm is a good threshold for a binary classification. The use of a threshold = 22.6 mm revealed a poorer performance, and 32 mm to be certainly not suitable for such a binary classification.

3.4 Application of the predictive model to large spatial scales

Figure 7 shows the downstream variation in the grain size (D_{50}) as predicted by the Huber regression model on 10 bands (see section 3.3) along 300 km of the Po River.

The model was applied using the reflectance values of Sentinel 2 data, collected on the 14th of September 2020. We can indeed reasonably assume that there is not a significant change in the gravel-sand transition position within the time of three years.

Model application shows a significant, abrupt decrease in the surface sediment grain size in the Po River around 140 km downstream from Torino, just below the confluence with the Ticino River. Here, over a relatively short downstream distance, sediment bars change from being gravel-dominated to sand-dominated. This gravel-sand transition has been verified also in the field.

17

Two wide sediment size distributions are well distinguishable upstream and downstream the gravel-sand transition, the former features a modal value around 28 mm, whereas the latter around 0.1 mm. Regarding the gravel bar sampled in 2018 upstream the Ticino River confluence, the UAV-based ground truth data (sitebar P1, Figure 1) confirm the range predicted by the model, and the model seems to reasonably represent the observed grain size heterogeneity (within the total average error of ±8.4 mm). Close to the Ticino River confluence, the model identifies the gravel-sand transition. In this area it was expected to have an intervening reach, evidenced by a change in the channel morphology from wandering, gravel-dominated bed to sinuous, sand-dominated one. This morphological transition is clearly visible from Google satellite and confirmed in the technical report of the Autorità di Bacino del fiume Po, 2007. Moreover, a field assessment was conducted to validate model predictions and gravel sand transition detection. Figure 8 shows an example of a bar selected on the gravel sand transition zone, at around 10 km upstream the Ticino River confluence.

Figure 8 shows the grain size predicted by the model, the spatial distribution on the sediment bar and the frequency distribution of predicted values. Photos taken in the field confirm the spatial arrangement and the values predicted by the model. Usually, through the intervening reach, a bimodal bed material composition is expected (Sambrook Smith and Ferguson, 1995; Ferguson et al., 2011). As shown in the pictures, the surface material on the bar is alternately unimodal sand or gravel, and bimodal gravel-sand mixture. Areas covered by coarse surface layer with sand in the sub-surface are present on the bar head while sand surface and subsurface dominate downstream, where gravel patches are found only close to the water channel. Two sediment samples representative of the bimodal distribution found in the bar were collected (in May 2021) and sieved in the laboratory (total of 4.1 kg of gravel material and of 1.4 kg of sand). Results of the sieving show that the gravel sample features a D_{50} of 13.94 mm and the sand sample of 0.67. These values validate the prediction made by the model, accounting for the total error of ±8.4 mm.

Moving downstream the Ticino River confluence, in the sand dominated bars, it can be noticed that the D_{50} values predicted differ more considerably in terms of D_{50} variations from the (few) values derived from lab sieving of field samples (bars P2 and P3, Figure 1) . On the sand bars along this river reach, a small fraction of gravel is predicted by the model over a few pixels. A further field assessment was then conducted in May 2021, on a sand

18

dominated river bar, located downstream the Isola Serafini dam (see Fig. 7 for field assessment location).

As it can be seen from the histograms in Figure 9, most of the pixels are predicted as sand, and very few data are measured as greater than 15 mm. It can be noticed that the coarser particles (black color) predicted follow a specific spatial distribution pattern, being all located at the border of the bars, close to the water channel. This pattern is found for all sand bars selected along the Po River length. In Figure 9 is reported just a zoom of the bar examined in the field, as an example. The field campaign confirmed the grain size data distribution predicted and the presence of coarser material close to the river channel, as evident from the pictures. The occurrence of gravel in this river reach is in truth not surprising and is also confirmed in the technical report made by the Autorità di Bacino del Fiume Po, 2007.

4. DISCUSSION

4.1 Feasibility of orbital grain size mapping of sediment size classes from Sentinel-2 imagery

In this study we have demonstrated the existence of significant correlations between reflectance intensity in various bands of Sentinel 2 imagery and the D_{50} fractions of the surface sediment grain size. Robust predictive models were built, which allowed us to estimate particle size classes from fine sand to coarse gravel, by orbital data, within an error of ±8.4 mm. Orbital grain size mapping of sand- vs. gravel-dominated bars from Sentinel-2 data is possible because of the inverse relation between radiance values of satellite data and particle size dimension.

We are aware that remote sensing data (in the case of this study, Sentinel 2 multispectral data) are influenced by the surface roughness, which, under specific conditions, is proportional to particles size. However, the complexity of fluvial substrates and the uncontrolled conditions in the field make surface reflectance interpretation subject to uncertainties. Indeed, beyond surface roughness, additional factors influence the spectral response of different types of substrates. Swain and Davis (1978), by studying reflectance properties of 240 types of soils, showed that all soils have a typical reflectance shape that varies in a quite large range, depending on soil texture (percentage of sand, silt and clay), soil moisture content (dry, moist, saturated), organic matter content, iron-oxide content, lithology and surface roughness. However, based on the choice of the sites made in our study (unvegetated, homogeneous and dry sediment bars, located in different geological context), and on the criteria followed for Sentinel 2 data download (days with no precipitation in the previous three days), we proceeded with this analysis to test the potential of the dataset collected to discriminate between finer and coarser particles – thus to see if the influence of surface roughness is strong enough to allow for that.

The spectral analysis made followed two approaches: firstly, we plotted the spectral signature of each site (by averaging the reflectance values of all pixels belonging to a sediment bar); secondly, we plotted the spectral signature of five sediment classes (by mixing the values coming from all sediment bars and averaging the reflectance values of all pixels belonging to a sediment class). The first plot (Figure 5a) showed that sites composed of sand particles (P2, P3, Figure 1) have the highest reflectance values and can be well discriminated from the others in the NIR and SWIR region. In the VIS region, instead, the spectral signatures are all very closed between each other. Indeed, for these wavelengths the inverse correlation of diameter and reflectance is less strong (as also confirmed from our results reported in Table 4). Notably, the sediment bars selected on the Bonamico River, featured by a D_{50} of 35 mm, have a lower spectral signature over the whole spectrum, in comparison to the other sites (B1, B2; Fig. 5a). This result is explained by accounting for the different factors that influences spectral response of soils (Swain and Davis 1978). Firstly, lithology plays an important role: the Bonamico River is characterized by a mixture in the lithological conditions (substrate dominated by dark metamorphic and sedimentary rocks) which is substantially different to the other study rivers (mainly dominated by lighter-colored metamorphic rocks), as also testified by the different orogenic processes that generate the geomorphology of the areas. Moreover, the Bonamico River is located in southern Italy, where environmental conditions (climatic, hydrological) are significantly different in comparison to the northern sites. The second plot (Fig. 5b) is referred to all the dataset collected, split into sediment classes. Results show that different sediment classes have well distinguishable spectral signatures, as far as we move towards longer wavelength. Again, the inverse correlation is stronger in the NIR and SWIR region, as expected from literature (Pilorget et al., 2016, Carson et al., 2015, Black et al., 2014) as well as, later, confirmed by our results (Table 4). The fact that, by mixing the dataset collected in the different sites, thus mixing different lithology and environmental conditions, particles sizes are distinguishable confirms that besides many parameters that influence

20

reflectance response, surface roughness of unvegetated, homogeneous, exposed and dry sediment river bars affect Sentinel-2 data enough to discriminate different sediment classes. Thus, these results indicate that surface roughness is one of the main parameters that affect the soil spectral signature, despite the uncontrolled factors that influence the overall reflectance. In this study we did not quantify the influence of each factor but we carefully selected the data to isolate as much as possible the effect of surface roughness over the others.

Spectral signatures analysis results were encouraging and confirmed the hypothesis made at the beginning of the study. We then calibrated linear and no linear models. All calibrated models showed a very high correlation (R^2) which ranges from as high as 0.98 for RF to 0.92 for Huber Regression, using the D_{50}. The latter model was chosen for further investigations. Indeed, despite slightly lower R^2 linear models rarely overfit and the Huber regression is thus preferable. Indeed, when we applied the RF to the entire Po, it generated trends with peaks and high non-linearities compared to smoother paths of the Huber Regressor. We believe this is due to overfitting issues of RF and then chose the Huber Regression for the Po case study application.

The most important bands resulting from the Huber regression model are those in the SWIR and NIR region, consistently with previous studies of Pilorget et al. (2016), Carson et al. (2015), Black et al. (2014) as well as the preliminary analysis made on the spectral signatures. Moreover, the negative coefficients appearing in single band models confirm that the physical effect of an inverse correlation between grain size and reflectance values of Sentinel 2 (Table 4) is likely the most influential physical processes to be captured (again, over the other factors that influence the spectral response of soils, in uncontrolled field conditions). The selected multiple linear regression model features some bands with a positive coefficient, notably bands in the same spectral region (because of the higher correlation between them). It is likely that those bands, appearing with positive sign, are related to the other factors that influence reflectance response, such as lithological or climate conditions. We also trained models with selected combinations of different bands but, so far, we argue that it is still too early to identify an optimal configuration of bands leading to a so-called 'best' predictive model and we proceeded with the 10 bands model as it achieved the best performance both in model training and application.

Logistic regression shows that the binary classification of particles lower and greater the threshold of 2 mm performed very well. The performance metric precision account for

21

0.85, the accuracy metric is 0.91. This confirms the first statement made that orbital grain size mapping from Sentinel 2 data is possible in terms of sand vs gravel classes, thus leading to a binary classification of sand versus gravel dominated river segments.

When applied to the 300 km of the Po River, our model prediction illustrates two contrasting, long river segments, two upstream and downstream of the Ticino River confluence (Figure 7). Data collected in 2018 on the gravel dominated bars and the field assessments carried out confirmed the predicted values and the identification of the gravel-sand transition (Figure 8) where a change in the channel morphology from wandering, gravel-dominated bed to sinuous, sand-dominated one is evident. Field campaign conducted on the sand dominated bars confirmed presence the of coarser material close to the river channel as predicted by the model (Figure 9). Indeed, as reported in the technical report made by the Autorità di Bacino del Fiume Po, 2007, along this river length, several important tributaries coming from the Apennines Mountain chain, such as Enza, Trebbia, Taro, bring coarse material and high sediment supply to the main channel. However, because of the deep and narrow channel, the river channel is sinuous, with alternate sand bars. The coarser material coming from the tributaries is likely transported at the bottom of the water channel. Its presence is revealed on the sand dominated bars by surface patches of coarser material, close to the water channel. Coarser material close to the river channel is predicted by the model in almost all sand-dominated bars. Explanation of the gravel predicted in these areas may also be linked to other factors such as the presence of higher soil moisture water content, grassy vegetation, standed woody material, and silt patches which characterize such transitional zones, thus influencing their surface spectral response.

The D_{84} percentile, which is typically used to predict hydraulic roughness in rivers, was also tested, and the results obtained were similar but with a slightly lower performance in terms of prediction robustness in the texture-based model calibrated.

Further work is needed to investigate how the different grain size percentiles are predicted in conditions other than those explored in this study, e.g., coarser sediments bars. However, we think that to derive a complete grain size distribution, Sentinel 2 satellite is not a suitable technology. Uncertainty and model limitations found in this work suggest that differences in bands' reflectance generated by varying grain sizes, roughness, and texture detectable from Sentinel 2 allow for a broad estimation of mean grain size - e.g., transitions from gravel to sand, and in future studies we may enlarge to the difference

22

between sand, gravel, and sand-gravel mixed patches (as already demonstrated using satellite radar data in Purinton and Bookhagen 2020), and boulder to gravel - but not for grain size distribution determination.

There are also constraints and limitations in the method which need to be taken into consideration. Sentinel 2 pixels need to be selected carefully based on specific criteria: i) satellite images need to be acquired on days not close to rainfall events since surface wetness influences reflectance values; ii) the Sentinel 2 pixel needs to capture a zone of bare sediment, homogeneous in terms of particle size and with no vegetation or water patches in the 10x10m analyzed area. Filters are indeed needed to delete contaminated pixels of water/vegetation and separate bright patches where the intensity is driven by sub-pixel scale vegetation from those patches where the intensity is driven by finer particle sizes. This condition is not always easy to meet. In this work we used the Fuzzy classifier outputs (Carbonneau et al. 2020) by setting the 95% value as a threshold. Other thresholds were tested and worked well but we preferred to remain conservative. Moreover, we chose to use computationally expensive super-resolution to get the best possible results from the fuzzy classifier. However, a simplified fuzzy model, generated only with the native 10 m Sentinel 2 bands 2, 3, 4 and 8, could be used instead (as demonstrated in Carbonneau et al., 2020), thus bypassing the need for the computationally expensive super-resolution. Moreover, other classifiers can be used to isolate sediment pixels only, also exploiting other technologies (e.g. Synthetic Aperture RADAR (SAR) for soil moisture content estimation).

The spatial resolution of Sentinel 2 data (10 m) poses a clear limitation for our approach. In fact, we think this methodology is reliably applicable only to rivers having exposed bars larger > 100 m^2. Therefore, our approach can be useful in relatively large rivers (>50-100 m) featuring reach-scale morphologies characterized by relatively large bars exposed at low flows, such as braided, wandering and sinuous with alternate bars typologies.

Another crucial aspect of the study is the atmospheric correction step to avoid atmospheric interference. Indeed, the scale of intensity changes that are caused by particle size variations could conceivably be completely masked by a poor atmospheric correction. In this study we used atmospherically corrected products of Sentinel 2 available as level 2A products. Moreover, model calibration was tested using products downloaded from the Theia catalogue, resulting from the use of the MACCS-ATCOR Joint Algorithm (MAJA) for the atmospheric correction (Lonjon et al., 2016), and the performance were comparable.

23

This further analysis gives more strength to our outputs since we can exclude that our outcomes are strictly dependent on the atmospheric correction type conducted.

4.3 Future Developments

New model calibration would be useful to give more robustness to the model and test it on sediment classes not included in this work (notably from 1 to 10 mm and particles in the range of pebbles/boulders). The model was indeed calibrated using grain size data up to coarse gravel, thus its applicability is valid in such grain size range. Any particles greater than coarse gravel class is not considered by the model, thus resulting in a possible underestimation of particles greater than the range considered. Future studies should investigate the potential of our approach by enlarging the grain size dataset and testing other satellites data (e.g. radar, Purinton and Bookhagen, 2020 and hyperspectral) to be used in combination with the multispectral data. Specifically, for coarser sediments, we expect that the use of radar data (electromagnetic range of the microwave), such as Sentinel 1, can be a technology to be explored. With the use of a low-cost commercial drone and calibration with the grain size mapping methods of Carbonneau et al. (2018), Woodget et al. (2018), grain dataset enlargement will require little effort in terms of time and costs. A data-driven approach able to measure grain size distributions from georeferenced UAV images on entire river bars, centered on linear regression model such that used in this work or more complex deep learning model such as convolutional neural network (Lang et al., 2021) will also allow for rapidly enlarge the dataset.

The ability of the model to reproduce large-scale downstream fining patterns, including gravel-sand dominated bars identification, was shown for the Po River. Model application was made on a date (14th of September 2020) selected with good hydrological and climate conditions, in a year (2020) in between 2018 and 2021 (date of the field work activities and model training). Other dates were also tested in 2018 and 2021 and the reproduced grain size variations are comparable (e.g. gravel sand transition identification) and follow the same explanations presented. Future analysis will apply the model in several dates to study the seasonal/annual trends. The gravel sand transition identification is a main finding of the model application and show the potential of this model in mapping and monitoring river processes at the catchment scale. Being able to map grain size classes in the range of sand and gravel at the catchment scale and to detect transitional zones through time can support river processes understanding (Smith and Ferguson 1995, Knighton, 1999;

24

Ferguson, 2003; Topping et al., 2018, Frings, 2011, Venditti and Church 2014) and answer questions such as: Where is the gravel-sand transition and what is its morphology? Which factors are causing a change in sediment composition and/or in the transition to migrate downstream/upstream?

Given the open-access nature of Sentinel 2 data and the high temporal frequency, the method can be applied through time and to other river systems to measure long-term changes in grain size classes in the range of gravel and sand, along hundreds of kilometers of river lengths. Mapping these precious data at such large temporal and spatial scale is fundamental to integrate emerging network-scale global monitoring and modeling (Pekel et al., 2016; Allen and Pavelsky 2018, Mouyen et al., 2018, Tangi et al. 2019, Schmitt et al., 2019) and to support water-management decision-making.

Finally, this approach can find novel application on the grain size data characterization of other open natural environment where an automatized sediment composition characterization is meaningful for earth surface processes understanding. New perspectives on natural environment both in plain and mountain areas (Williams and Brierley 2019, Coviello et al., 2021, Trevisani and Cavalli 2016, Kofler et al., 2021) are worth to be investigated in the future.

5. CONCLUSION

We believe that the most important contribution of this paper is the first orbital grain size mapping of sediment classes from freely available Sentinel 2 data. This is a fundamentally new area of remote sensing which will allow for grain size characterization of sand and gravel sediment classes of very long reaches (>100 km) at very low cost.

In this paper, we used near-ground UAV imagery to calibrate robust linear correlations between the grain sizes, D_{50} (mm), on dry exposed river bars and reflectance values in Sentinel 2 imagery. We obtained statistically significant predictive models for D_{50}, able to predict, within an error of about 10 mm, sediment grain size classes in the range of sand and gravel. Used in prediction, this model reproduced the expected downstream fining trends for a 300 km long stretch of the River Po in Northern Italy, notably identifying the gravel sand transition occurring along the river length.

ACKNOWLEDGEMENTS

25

This work was performed in the framework of the “IRIS – Italian Research and development Initiative for Spaceborne river monitoring”, : https://www.isprambiente.gov.it/pre_meteo/idro/idro.html#HabitatMapping, funded in the context of the Italian Space Agency-ISPRA initiative “Habitat Mapping”. The authors are grateful to the EU Copernicus Programme for providing Sentinel 2 L2A data and to Theia for making available MAJA corrected Sentinel 2 data. We thank Dr. Martina Bussettini, Dr. Stefano Mariani, Mr. Marco Casaioli and Ms. Francesca Piva for DJI Phantom 4 Pro and Trimble R10 RTK-GPS acquisitions during ground fields. We also thank colleagues Andrea Andreoli and Velio Coviello for the support in the field and in the laboratory. Finally, thanks to Prof Andrea Francesco Castelletti for the support at the beginning of this work at Politecnico di Milano, Milan, Italy. B. Belletti contribution was in part supported by the EUR H2O’Lyon (ANR-17-EURE-0018).

26

References

Allen GH, Pavelsky TM. 2018. Global extent of rivers and streams. Science [online] Available from: https://www.science.org/doi/abs/10.1126/science.aat0636 (Accessed 3 September 2021)

Anon. n.d. Combining medium and coarse spatial resolution satellite data to improve the estimation of sub-pixel NDVI time series - ScienceDirect [online] Available from: https://www.sciencedirect.com/science/article/pii/S0034425707001563?casa_token=nplTUF47jbUAAAAA:B3jtg8yXpXu056hAQrrugqzTIdCmvF4HdyFr64gegh-YDaywtqXKxmFQJnbipbfW_in2lQNZhQ (Accessed 8 September 2021)

Autorità di bacino del fiume Po. 2007. Aggiornamento delle analisi morfologiche e del bilancio del trasporto solido dell'asta del fiume Po da confluenza Stura di Lanzo all'incile del delta (periodo 2002 – 2005) e report di valutazione

Black M, Carbonneau P, Church M, Warburton J. 2014. Mapping sub-pixel fluvial grain sizes with hyperspatial imagery. Sedimentology 61 : 691–711. DOI: 10.1111/sed.12072

Brodu N. 2017. Super-Resolving Multiresolution Images With Band-Independent Geometry of Multispectral Pixels. IEEE Transactions on Geoscience and Remote Sensing 55 : 4610–4617. DOI: 10.1109/TGRS.2017.2694881

Buscombe D, Masselink G. 2009. Grain-size information from the statistical properties of digital images of sediment. Sedimentology 56 : 421–438. DOI: 10.1111/j.1365-3091.2008.00977.x

Buscombe D, Rubin DM, Warrick JA. 2010. A universal approximation of grain size from images of noncohesive sediment. Journal of Geophysical Research: Earth Surface 115 : F02015. DOI: 10.1029/2009JF001477

Busetto L, Meroni M, Colombo R. 2008. Combining medium and coarse spatial resolution satellite data to improve the estimation of sub-pixel NDVI time series. Remote Sensing of Environment 112 : 118–131. DOI: 10.1016/j.rse.2007.04.004

Carbonneau PE, Bizzi S, Marchetti G. 2018. Robotic photosieving from low-cost multirotor sUAS: a proof-of-concept. Earth Surface Processes and Landforms : n/a-n/a. DOI: 10.1002/esp.4298

 27

Carbonneau PE, Belletti B, Micotti M, Lastoria B, Casaioli M, Mariani S, Marchetti G, Bizzi S. 2020. UAV-based training for fully fuzzy classification of Sentinel-2 fluvial scenes. Earth Surface Processes and Landforms 45 : 3120–3140. DOI: 10.1002/esp.4955

Carbonneau PE, Bergeron N, Lane SN. 2005a. Automated grain size measurements from airborne remote sensing for long profile measurements of fluvial grain sizes. Water Resources Research 41 : W11426. DOI: 10.1029/2005WR003994

Carbonneau PE, Bergeron NE, Lane SN. 2005b. Texture-based image segmentation applied to the quantification of superficial sand in salmonid river gravels. Earth Surface Processes and Landforms 30 : 121–127. DOI: 10.1002/esp.1140

Carbonneau PE, Lane SN, Bergeron NE. 2004. Catchment-scale mapping of surface grain size in gravel bed rivers using airborne digital imagery. Water Resources Research 40 : W07202. DOI: 10.1029/2003WR002759

Carson T, Bachmann CM, Salvaggio C. 2015. Soil signature simulation of complex mixtures and particle size distributions. Optical Engineering 54 : 094103. DOI: 10.1117/1.OE.54.9.094103

Cavalli, M, Tarolli, P., Marchi, L., and Dalla Fontana, G 2008. The effectiveness of airborne LiDAR data in the recognition of channel-bed morphology, CATENA, 73, 249–260, doi:10.1016/j.catena.2007.11.001

Chappell, A. and Heritage, G.L., 2007. Using illumination and shadow to model aerodynamic resistance and flow separation: An isotropic study. Atmospheric Environment, 41(28), 5817-5830.

Coviello V, Theule JI, Crema S, Arattano M, Comiti F, Cavalli M, LucÍa A, Macconi P, Marchi L. 2020. Combining Instrumental Monitoring and High-Resolution Topography for Estimating Sediment Yield in a Debris-Flow Catchment. Environmental and Engineering Geoscience 27 : 95–111. DOI: 10.2113/EEG-D-20-00025

Detert M, Weitbrecht V. 2012. Automatic object detection to analyze the geometry of gravel grains – a free stand-alone tool. River Flow 2012 : 595–600.

Downing JA, Cole JJ, Duarte CM, Middelburg JJ, Melack JM, Prairie YT, Kortelainen P, Striegl RG, McDowell WH, Tranvik LJ. 2012. Global abundance and size distribution of streams and rivers. Inland Waters 2 : 229–236. DOI: 10.5268/IW-2.4.502

28

Dugdale SJ, Carbonneau PE, Campbell D. 2010. Aerial photosieving of exposed gravel bars for the rapid calibration of airborne grain size maps. Earth Surface Processes and Landforms 35 : 627–639. DOI: 10.1002/esp.1936

Fausch KD, Torgersen CE, Baxter CV, Li HW. 2002. Landscapes to Riverscapes: Bridging the Gap between Research and Conservation of Stream Fishes. BioScience 52 : 483–498. DOI: 10.1641/0006-3568(2002)052[0483:LTRBTG]2.0.CO;2

Ferguson R, Hoey T, Wathen S, Werritty A. 1996. Field evidence for rapid downstream fining of river gravels through selective transport. Geology 24 : 179–182. DOI: 10.1130/0091-7613(1996)024<0179:FEFRDF>2.3.CO;2

Ferguson RI, Bloomer DJ, Church M. 2011. Evolution of an advancing gravel front: observations from Vedder Canal, British Columbia. Earth Surface Processes and Landforms 36 : 1172–1182. DOI: 10.1002/esp.2142

Frings RM, Ottevanger W, Sloff K (C. J. 2011. Downstream fining processes in sandy lowland rivers. Journal of Hydraulic Research 49 : 178–193. DOI: 10.1080/00221686.2011.561000

Graham DJ, Reid I, Rice SP. 2005. Automated Sizing of Coarse-Grained Sediments: Image-Processing Procedures. Mathematical Geology 37 : 1–28. DOI: 10.1007/s11004-005-8745-x

Graham DJ, Rollet A-J, Piégay H, Rice SP. 2010. Maximizing the accuracy of image-based surface sediment sampling techniques. Water Resources Research 46 DOI: 10.1029/2008WR006940 [online] Available from: http://onlinelibrary.wiley.com/doi/10.1029/2008WR006940/full (Accessed 5 February 2018)

Grohmann, C. H., Smith, M. J., and Riccomini, C.: Multiscale Analysis of Topographic Surface Roughness in the Midland Valley, Scotland, IEEE Geosci. Remote S., 49, 1200–1213, doi:10.1109/TGRS.2010.2053546, 2011.

Gumiero B, Surian N, Maiolini B, Boz B, Rinaldi M, Moroni F. 2009. Chapter 12 - The Italian Rivers. In Rivers of Europe , Tockner K, Uehlinger U, and Robinson CT (eds). Academic Press: London; 467–495. [online] Available from: https://www.sciencedirect.com/science/article/pii/B9780123694492000126 (Accessed 2 September 2021)

29

Hapke B. 1984. Bidirectional reflectance spectroscopy: 3. Correction for macroscopic roughness. Icarus 59 : 41–59. DOI: 10.1016/0019-1035(84)90054-X

Heritage, G.L. and Milan, D.J., 2009. Terrestrial laser scanning of grain roughness in a gravel-bed river. Geomorphology, 113(1-2), 4-11.

Hodge, R., Brasington, J. and Richards, K., 2009. In situ characterization of grain-scale fluvial morphology using Terrestrial Laser Scanning. Earth Surface Processes and Landforms, 34(7), 954-968.

Knighton AD. 1999. The gravel–sand transition in a disturbed catchment. Geomorphology 27 : 325–341. DOI: 10.1016/S0169-555X(98)00078-6

Kofler C, Mair V, Gruber S, Todisco MC, Nettleton I, Steger S, Zebisch M, Schneiderbauer S, Comiti F. 2021. When do rock glacier fronts fail? Insights from two case studies in South Tyrol (Italian Alps). Earth Surface Processes and Landforms 46 : 1311–1327. DOI: 10.1002/esp.5099

Lang N, Irniger A, Rozniak A, Hunziker R, Wegner JD, Schindler K. 2021. GRAINet: mapping grain size distributions in river beds from UAV images with convolutional neural networks. Hydrology and Earth System Sciences 25 : 2567–2597. DOI: 10.5194/hess-25-2567-2021

Marchetti M. 2002. Environmental changes in the central Po Plain (northern Italy) due to fluvial modifications and anthropogenic activities. Geomorphology 44 : 361–373. DOI: 10.1016/S0169-555X(01)00183-0

Mouyen M, Longuevergne L, Steer P, Crave A, Lemoine J-M, Save H, Robin C. 2018. Assessing modern river sediment discharge to the ocean using satellite gravimetry. Nature Communications 9 : 3384. DOI: 10.1038/s41467-018-05921-y

Nash DB, Conel JE. 1974. Spectral reflectance systematics for mixtures of powdered hypersthene, labradorite, and ilmenite. Journal of Geophysical Research (1896-1977) 79 : 1615–1621. DOI: 10.1029/JB079i011p01615

Pedregosa F et al. n.d. Scikit-learn: Machine Learning in Python. MACHINE LEARNING IN PYTHON : 6.

Pekel J-F, Cottam A, Gorelick N, Belward AS. 2016. High-resolution mapping of global surface water and its long-term changes. Nature 540 : 418–422. DOI: 10.1038/nature20584

30

Pilorget C, Fernando J, Ehlmann BL, Douté S. 2015. Photometry of particulate mixtures: What controls the phase curve? Icarus 250 : 188–203. DOI: 10.1016/j.icarus.2014.11.036

Pilorget C, Fernando J, Ehlmann BL, Schmidt F, Hiroi T. 2016a. Wavelength dependence of scattering properties in the VIS–NIR and links with grain-scale physical and compositional properties. Icarus 267 : 296–314. DOI: 10.1016/j.icarus.2015.12.029

Pilorget C, Fernando J, Ehlmann BL, Schmidt F, Hiroi T. 2016b. Wavelength dependence of scattering properties in the VIS–NIR and links with grain-scale physical and compositional properties. Icarus 267 : 296–314. DOI: 10.1016/j.icarus.2015.12.029

Pilorget C, Vincendon M, Poulet F. 2013. A radiative transfer model to simulate light scattering in a compact granular medium using a Monte–Carlo approach: Validation and first applications. Journal of Geophysical Research: Planets 118 : 2488–2501. DOI: 10.1002/2013JE004465

Pitlick J, Mueller ER, Segura C, Cress R, Torizzo M. 2008. Relation between flow, surface-layer armoring and sediment transport in gravel-bed rivers. Earth Surface Processes and Landforms 33 : 1192–1209. DOI: 10.1002/esp.1607

Pizzuto JE. 1995. Downstream Fining in a Network of Gravel-Bedded Rivers. Water Resources Research 31 : 753–759. DOI: 10.1029/94WR02532

Purinton B, Bookhagen B. 2019. Introducing PebbleCounts: a grain-sizing tool for photo surveys of dynamic gravel-bed rivers. Earth Surface Dynamics 7 : 859–877. DOI: 10.5194/esurf-7-859-2019

Purinton B, Bookhagen B. 2020. Multiband (X, C, L) radar amplitude analysis for a mixed sand- and gravel-bed river in the eastern Central Andes. Remote Sensing of Environment 246 : 111799. DOI: 10.1016/j.rse.2020.111799

Rice SP, Church M. 2001. Longitudinal profiles in simple alluvial systems. Water Resources Research 37 : 417–426. DOI: 10.1029/2000WR900266

Robinson DA, Friedman SP. 2005. Electrical conductivity and dielectric permittivity of sphere packings: Measurements and modelling of cubic lattices, randomly packed monosize spheres and multi-size mixtures. Physica A: Statistical Mechanics and its Applications 358 : 447–465. DOI: 10.1016/j.physa.2005.03.054

31

Rubin DM. 2004. A Simple Autocorrelation Algorithm for Determining Grain Size from Digital Images of Sediment. Journal of Sedimentary Research 74 : 160–165. DOI: 10.1306/052203740160

Sambrook Smith GH, Ferguson RI. 1995. The gravel-sand transition along river channels. Journal of Sedimentary Research 65 : 423–430. DOI: 10.1306/D42680E0-2B26-11D7-8648000102C1865D

Schmitt RJP, Bizzi S, Castelletti A, Opperman JJ, Kondolf GM. 2019. Planning dam portfolios for low sediment trapping shows limits for sustainable hydropower in the Mekong. Science Advances 5 : eaaw2175. DOI: 10.1126/sciadv.aaw2175

Smith, M.W., 2014. Roughness in the earth sciences. Earth-Science Reviews, 136, 202-225.

Surian N, Rinaldi M. 2003. Morphological response to river engineering and management in alluvial channels in Italy. Geomorphology 50 : 307–326. DOI: 10.1016/S0169-555X(02)00219-2

Tangi M, Schmitt R, Bizzi S, Castelletti A. 2019. The CASCADE toolbox for analyzing river sediment connectivity and management. Environmental Modelling & Software 119 : 400–406. DOI: 10.1016/j.envsoft.2019.07.008

Topping DJ, Mueller ER, Schmidt JC, Griffiths RE, Dean DJ, Grams PE. 2018. Long-Term Evolution of Sand Transport Through a River Network: Relative Influences of a Dam Versus Natural Changes in Grain Size From Sand Waves. Journal of Geophysical Research: Earth Surface 123 : 1879–1909. DOI: 10.1029/2017JF004534

Trevisani S, Cavalli M. 2016. Topography-based flow-directional roughness: potential and challenges. Earth Surface Dynamics 4 : 343–358. DOI: 10.5194/esurf-4-343-2016

Vázquez-Tarrío D, Borgniet L, Liébault F, Recking A. 2017. Using UAS optical imagery and SfM photogrammetry to characterize the surface grain size of gravel bars in a braided river (Vénéon River, French Alps). Geomorphology 285 : 94–105. DOI: 10.1016/j.geomorph.2017.01.039

Venditti JG, Church M. 2014. Morphology and controls on the position of a gravel-sand transition: Fraser River, British Columbia. Journal of Geophysical Research: Earth Surface 119 : 1959–1976. DOI: 10.1002/2014JF003147

 32

Verdú JM, Batalla RJ, Martínez-Casasnovas JA. 2005. High-resolution grain-size characterisation of gravel bars using imagery analysis and geo-statistics. Geomorphology 72 : 73–93. DOI: 10.1016/j.geomorph.2005.04.015

Verhoeye J, De Wulf R. 2002. Land cover mapping at sub-pixel scales using linear optimization techniques. Remote Sensing of Environment 79 : 96–104. DOI: 10.1016/S0034-4257(01)00242-5

Vincent Lonjou, Camille Desjardins, Olivier Hagolle, Beatrice Petrucci, Thierry Tremas, Michel Dejus, Aliaksei Makarau, Stefan Auer. 2016. MACCS-ATCOR joint algorithm (MAJA). presented at the Proc.SPIE. 19 October [online] Available from: https://doi.org/10.1117/12.2240935

Walt S van der, Schönberger JL, Nunez-Iglesias J, Boulogne F, Warner JD, Yager N, Gouillart E, Yu T. 2014. scikit-image: image processing in Python. PeerJ 2 : e453. DOI: 10.7717/peerj.453

Wentworth, K. “A scale of grade and class terms for clastic sediments”. The Journal of Geology, 1922.

Westoby MJ, Brasington J, Glasser NF, Hambrey MJ, Reynolds JM. 2012. ‘Structure-from-Motion’ photogrammetry: A low-cost, effective tool for geoscience applications. Geomorphology 179 : 300–314. DOI: 10.1016/j.geomorph.2012.08.021

Williams RD, Reid HE, Brierley GJ. 2019. Stuck at the Bar: Larger-Than-Average Grain Lag Deposits and the Spectrum of Particle Mobility. Journal of Geophysical Research: Earth Surface 124 : 2751–2756. DOI: 10.1029/2019JF005137

Woodget AS, Fyffe C, Carbonneau PE. 2018. From manned to unmanned aircraft: Adapting airborne particle size mapping methodologies to the characteristics of sUAS and SfM. Earth Surface Processes and Landforms 43 : 857–870. DOI: 10.1002/esp.4285

33

Figures Captions

Figure 1. Study area. Location of the 6 surveyed bars along the Po (P1, P2, P3), Sesia (S1) and Bonamico (B1, B2) rivers and a photo of each bar and their sediments. TMR, TMQ, TNQ and SWC represent the footprints of the Sentinel 2 tiles that cover the study sites.

Figure 2. The methodological workflow includes: the ground-truthing data collection carried out for gravel-dominated bars and for sand-dominated bars. Each step is applied to each sediment bar selected as study site, reported in figure 1. For each sediment bar the outcome is a grain size map generated at 10 m/pixel. This map is combined with Sentinel 2 multispectral data collected in the same site and used for Model Fitting. The Fuzzy logic classifier by Carbonneau et al. (2020) is used to isolate sediment pixels only. Afterwards, the model was applied on sediment river bars selected along 300 km of the Po River. Multispectral Sentinel 2 data are the input variable and the model results in grain size maps predicted in each sediment bar (selected exploiting the Fuzzy logic classifier).

Figure 3. Fuzzy logic classifier. Figure 3 a) shows, on the left, river corridor classified in the Fuzzy logic members, in a wandering reach, upstream the Ticino River confluence; on the right the same river reach on a Sentinel 2 image, where results of the model application (D_{50} predicted) are shown in a gray scale color in correspondence of Sentinel 2 pixel selected as sediment; Figure 3 b) shows the same as in a) on a sinuous river reach close downstream the Ticino River confluence, close to Isola Serafini dam.

Figure 4. The results of the texture-based model (gravel bars): a) plot of Dissimilarity (measured on 101x101 pixels window size) vs D_{50} (mm); b) plot of the observed vs predicted D_{50} values. Green shading accounts for the standard error of the regression line.

Figure 5. Sentinel-2 spectral signatures. a) spectral analysis of each site, featured by different median diameter: 34.9 mm P1 site, 32.8 mm B1 site, 42.4 mm S1 site, 0.43 mm P2 site, 0.35 mm P3 site, 42.3 mm B2 site. b) signature analysis of each sediment class. On the y axis are reported the radiance values, on the x axis the electromagnetic spectrum discretized according to the 10 Sentinel 2 bands available. Different colors are used to show the spectral signature of the different study sites (a) and of different grain size classes (b).

Figure 6. Observed versus predicted D_{50} for the Huber Regressor model with all bands as predictor variables. Reflectance values vs. D_{50} observed diameter. Each site is distinguishable by a different color.

Figure 7. Results of downstream fining modelling on 300 km of the Po River, from Torino city to Cremona city, using the Huber regression model with 10 bands. Blue points are the median diameter predicted in each pixel (Sentinel 2 dimension) belonging to sediment bars. Red diamonds refer to the D_{50} values measured by the ground-truthing methods. All pixels in each bar are assigned with a value for downstream distance. Below, a sketch of the Po River course is shown.

 34

Green diamonds show the location where an assessment was conducted to further validate the model prediction.

Figure 8. Field assessment on a river bar selected in the transition zone. On the left, grain size predicted expressed as frequency distribution as well as by gray color scale of the pixels (10x10 m) on the bar (image background from Google satellite). On the right, pictures taken in the field.

Figure 9. Field assessment on a sand dominated bar selected downstream Isola Serafini dam. On the left, grain size predicted expressed as frequency distribution as well as by gray color scale of the pixels (10x10 m) in the bar (image background from Google satellite). On the right, pictures taken in the field.

 35

Tables

Table 1. Ground truth data measured by photosieving technique (gravel samples) and sieving in the laboratory (sand samples). S1, site along the Sesia river; P1-P3, sites along the Po River; B1, B2, sites along the Bonamico.

Site	Area (km^2)	D_{50} (mm)
S1	0.06	42.4
P1	0.27	34.9
P2	0.22	0.43
P3	0.19	0.35
B1	0.25	32.8
B2	0.12	42.3

Table 2. Results for different modeling techniques for the train and test set. 10 bands used as predictor variables. MSE is Mean Squared Error; MAE is Mean Absolute Error.

All bands	*Train set*			*Test set*		
	R^2	MSE	MAE (mm)	R^2	MSE	MAE (mm)
Huber Regression	0.92	15.56	2.85	0.91	16.73	2.95
Random Forest	0.98	2.16	0.72	0.97	5.20	1.06
DNN	0.86	346.7	12.76	0.88	351.47	12.86

Table 3. Coefficients of the bands in the multiple linear regression model

B2	B3	B4	B5	B6	B7	B8	B8A	B11	B12
-193.1	104.0	59.2	242.7	196.4	127.9	-213.0	-36.98	41.78	-356.8

36

Table 4. Correlation of each band with the D50 diameter (mm) expressed as coefficient of correlation (R), coefficient of determination (R2), and related correlation coefficients.

	B2	B3	B4	B5	B6	B7	B8	B8A	B11	B12
R	-0.65	-0.54	-0.5	-0.56	-0.57	-0.6	-0.58	-0.61	-0.73	-0.81
R^2	0.3	0.06	0.07	0.09	0.1	0.2	0.2	0.2	0.4	0.6
Coeff	-315.4	-264.8	-234	-224.8	-221	-212.9	-199.6	-207.9	-164.3	-145.9

Table 5. Logistic regression results of the three thresholds (2, 22.6, 32 mm) selected for a binary classification of sand) and gravel particles in the dataset, following the Wentworth scale (Wentworth, 1922).

	D50 > 2 mm (predicted)	D50 < 2 mm (predicted)
D50 > 2 mm (actual)	348	86
D50 < 2 mm (actual)	0	486
	D50 > 22.6 mm (predicted)	D50 < 22.6 mm (predicted)
D50 > 22.6 mm (actual)	271	108
D50 < 22.6 mm (actual)	15	526
	D50 > 32 mm (predicted)	D50 < 32 mm (predicted)
D50 > 32 mm (actual)	0	59
D50 < 32 mm (actual)	0	861

37

Figures

38

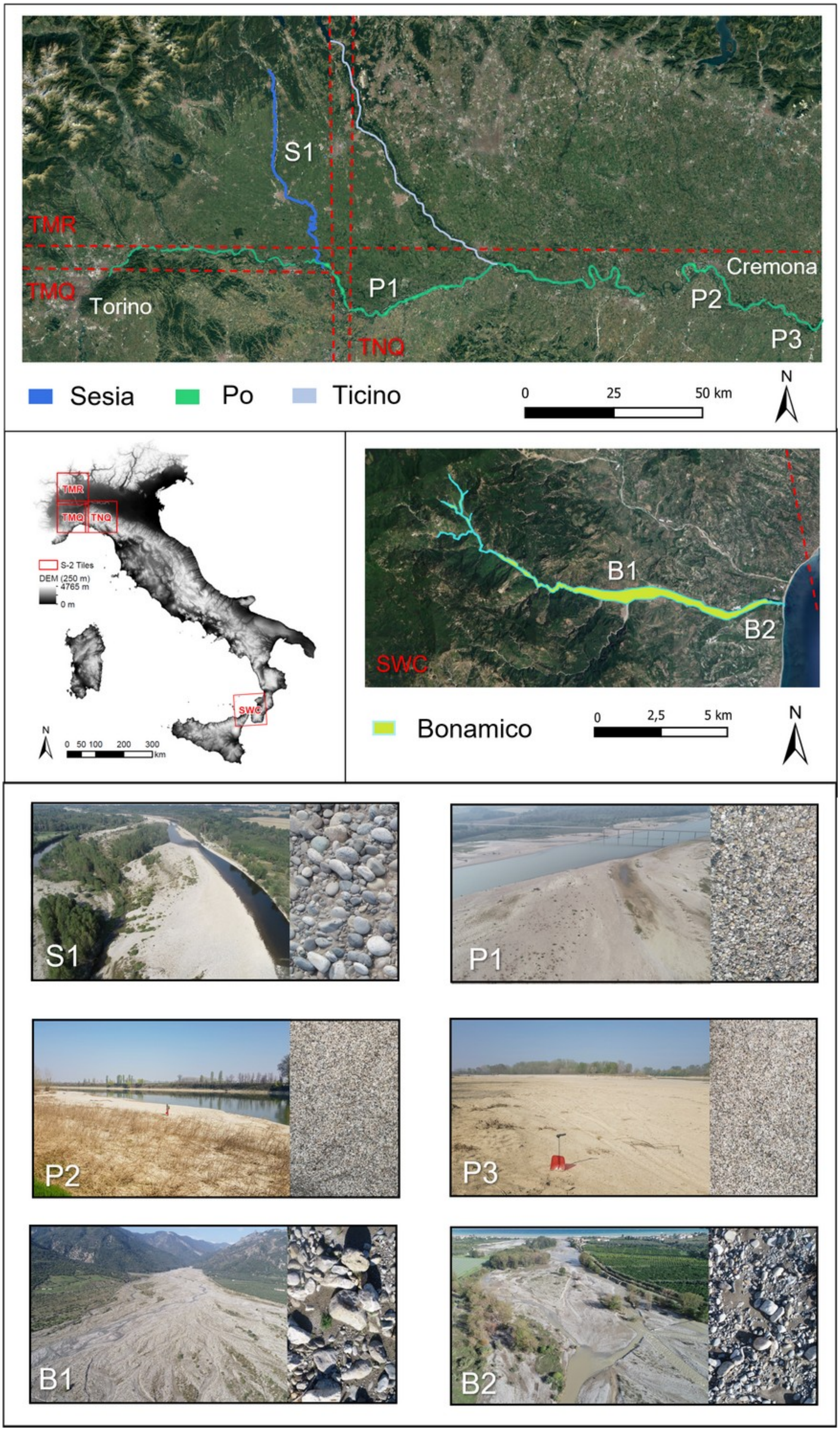
S1
TMR
TMQ
Torino
P1
TNQ
Cremona
P2
P3
Sesia
Po
Ticino
0
25
50 km
N
TMR
TMQ
TNQ
S-2 Tiles
DEM (250 m)
4765 m
0 m
SWC
N
0 50 100 200 300
km
B1
B2
SWC
Bonamico
0
2,5
5 km
N
S1
P1
P2
P3
B1
B2

39

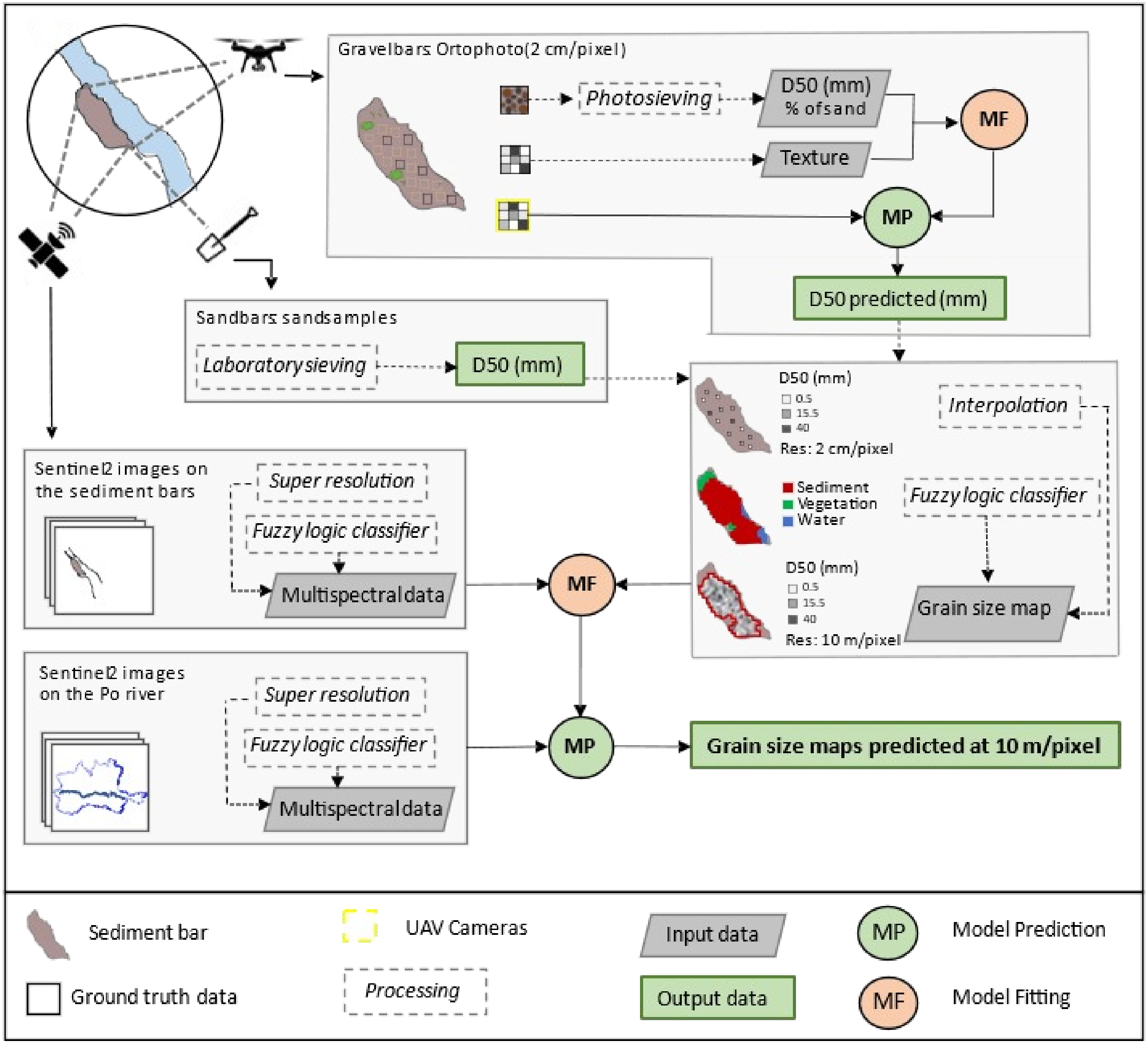
Gravelbars Ortophoto (2 cm/pixel)
Photosieving
D50 (mm)
% of sand
Texture
MF
MP
D50 predicted (mm)
Sandbars sand samples
Laboratory sieving
D50 (mm)
D50 (mm)
0.5
15.5
40
Res: 2 cm/pixel
Interpolation
Sediment
Vegetation
Water
Fuzzy logic classifier
D50 (mm)
0.5
15.5
40
Res: 10 m/pixel
Grain size map
Sentinel2 images on the sediment bars
Super resolution
Fuzzy logic classifier
Multispectral data
MF
Sentinel2 images on the Po river
Super resolution
Fuzzy logic classifier
Multispectral data
MP
Grain size maps predicted at 10 m/pixel
Sediment bar
Ground truth data
UAV Cameras
Processing
Input data
Output data
MP
Model Prediction
MF
Model Fitting

40

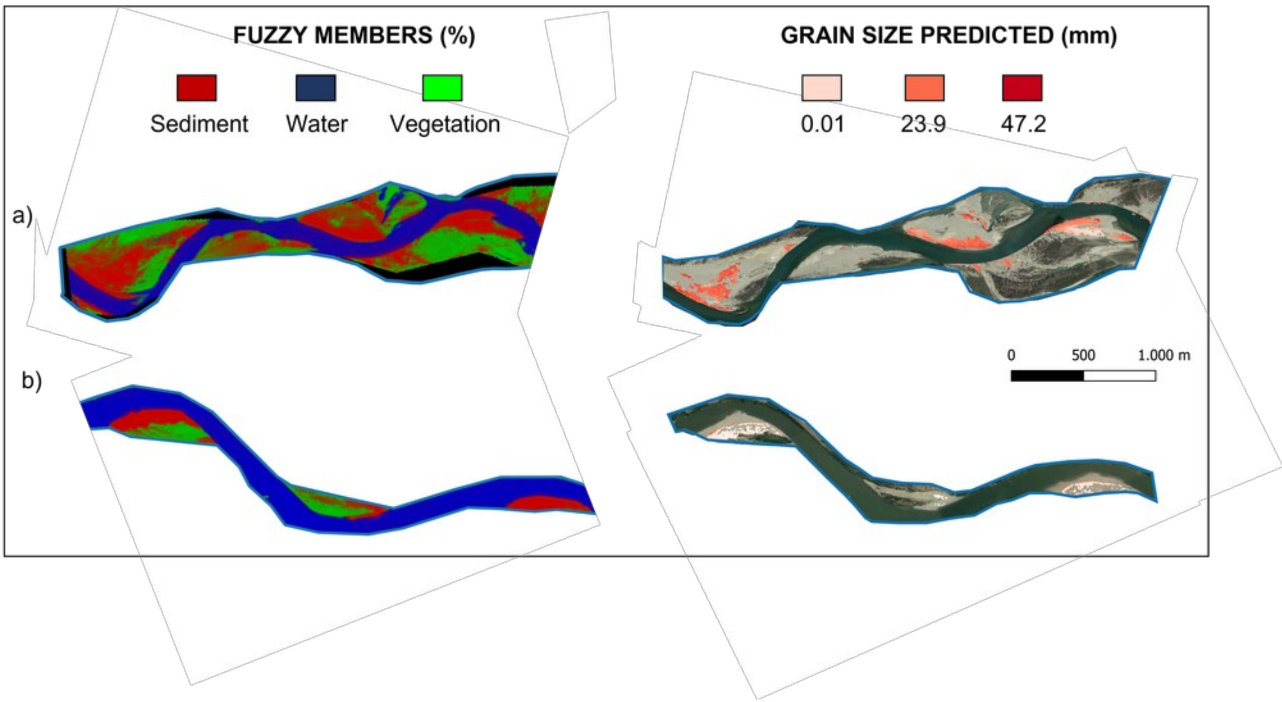
FUZZY MEMBERS (%)
Sediment
Water
Vegetation
GRAIN SIZE PREDICTED (mm)
0.01
23.9
47.2
a)
b)
0
500
1.000 m

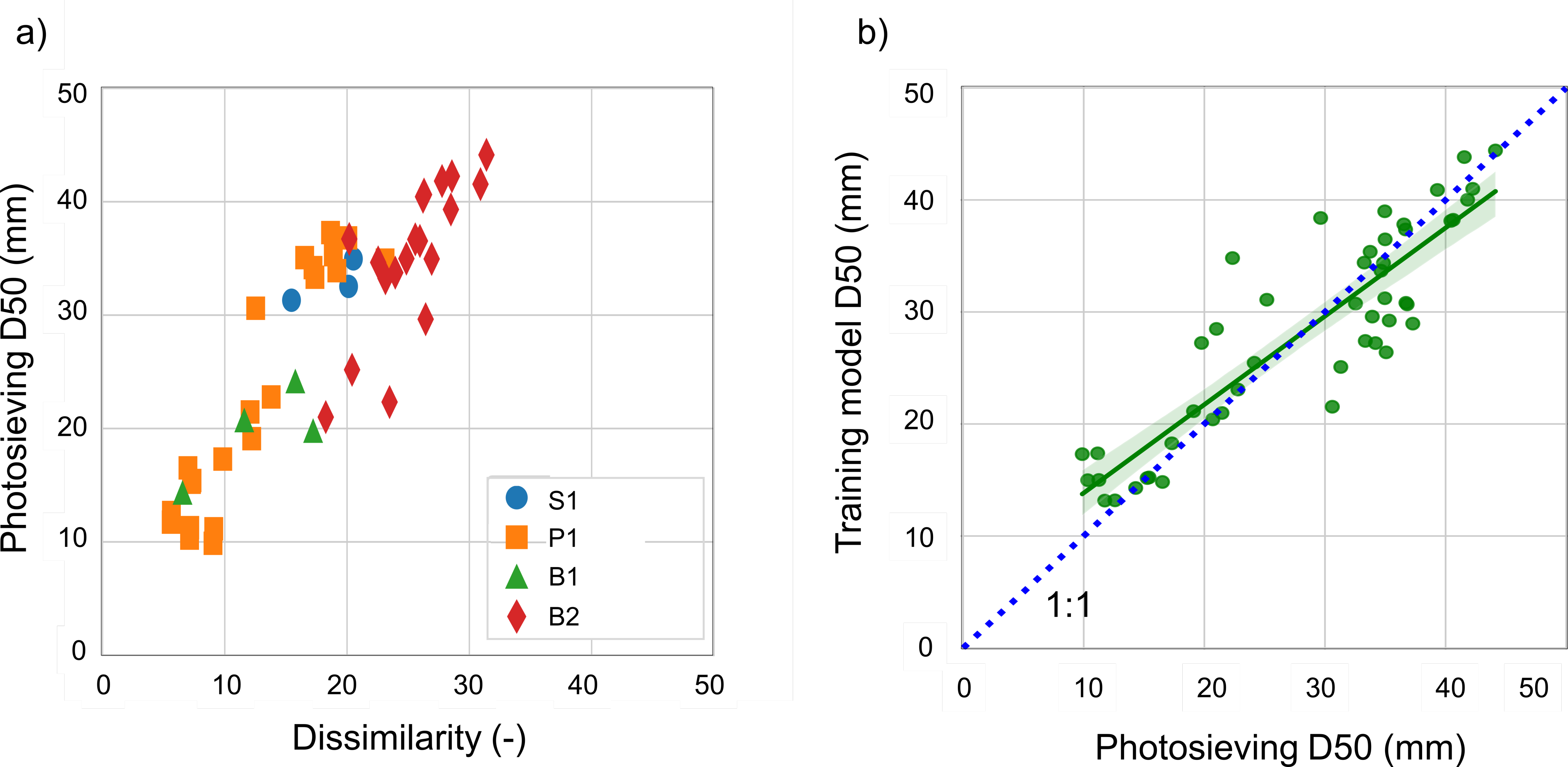

a)
b)
Photosieving D50 (mm)
Dissimilarity (-)
S1
P1
B1
B2
Training model D50 (mm)
Photosieving D50 (mm)
1:1
0
10
20
30
40
50

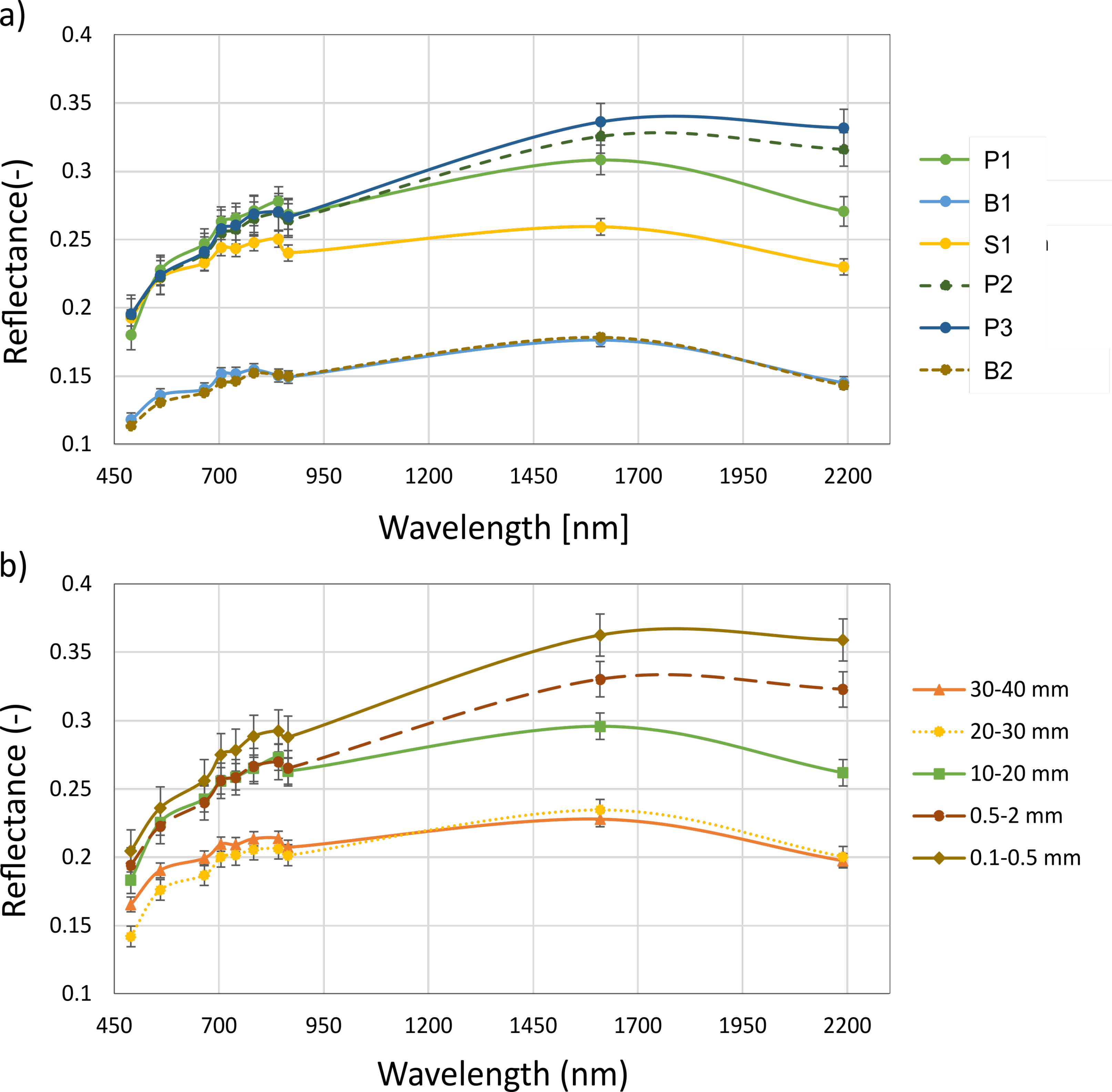
a)
Reflectance(-)
0.4
0.35
0.3
0.25
0.2
0.15
0.1
450
700
950
1200
1450
1700
1950
2200
Wavelength [nm]
P1
B1
S1
P2
P3
B2
b)
Reflectance (-)
0.4
0.35
0.3
0.25
0.2
0.15
0.1
450
700
950
1200
1450
1700
1950
2200
Wavelength (nm)
30-40 mm
20-30 mm
10-20 mm
0.5-2 mm
0.1-0.5 mm

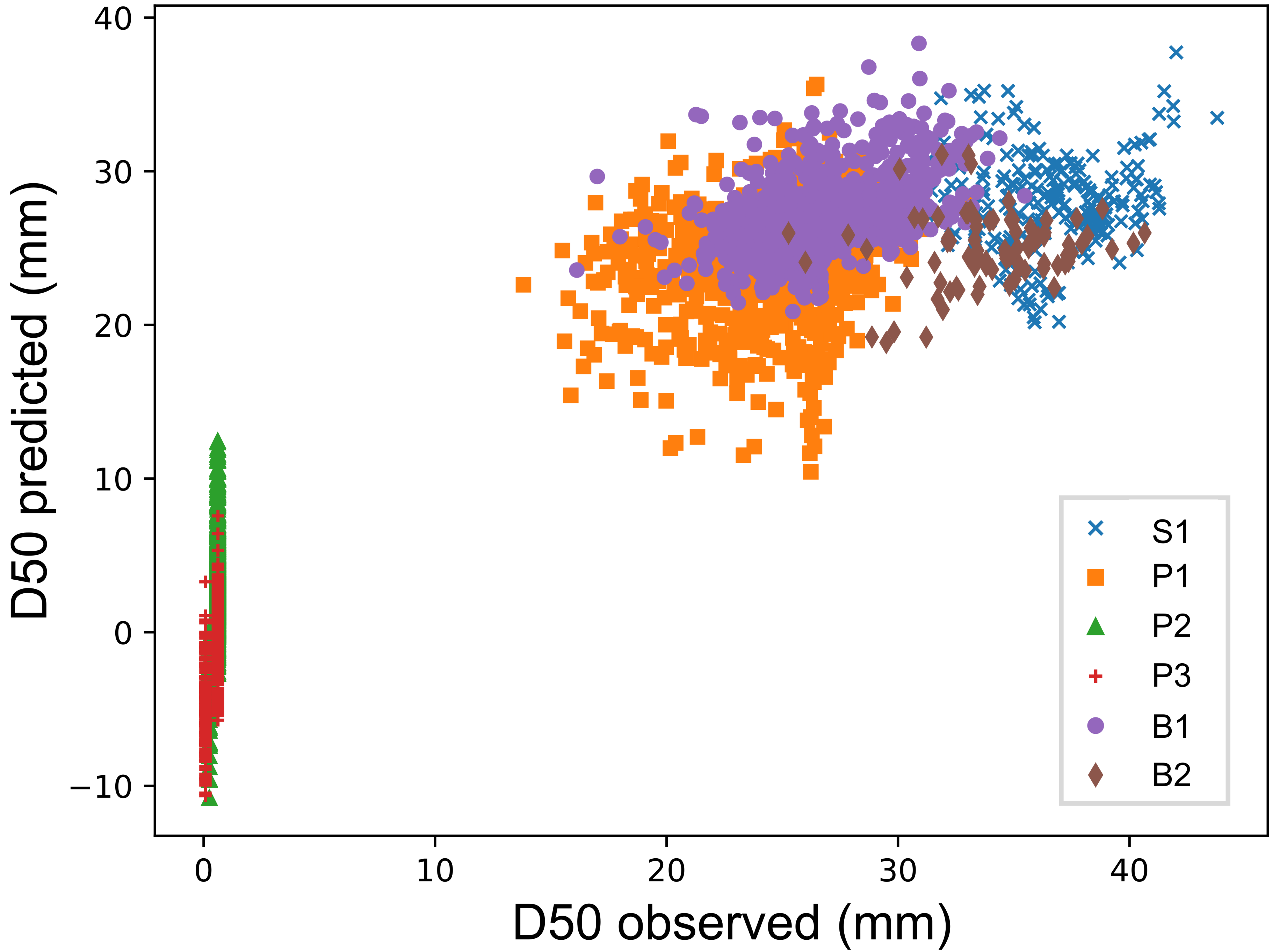
D50 predicted (mm)
D50 observed (mm)
40
30
20
10
0
−10
0
10
20
30
40
S1
P1
P2
P3
B1
B2

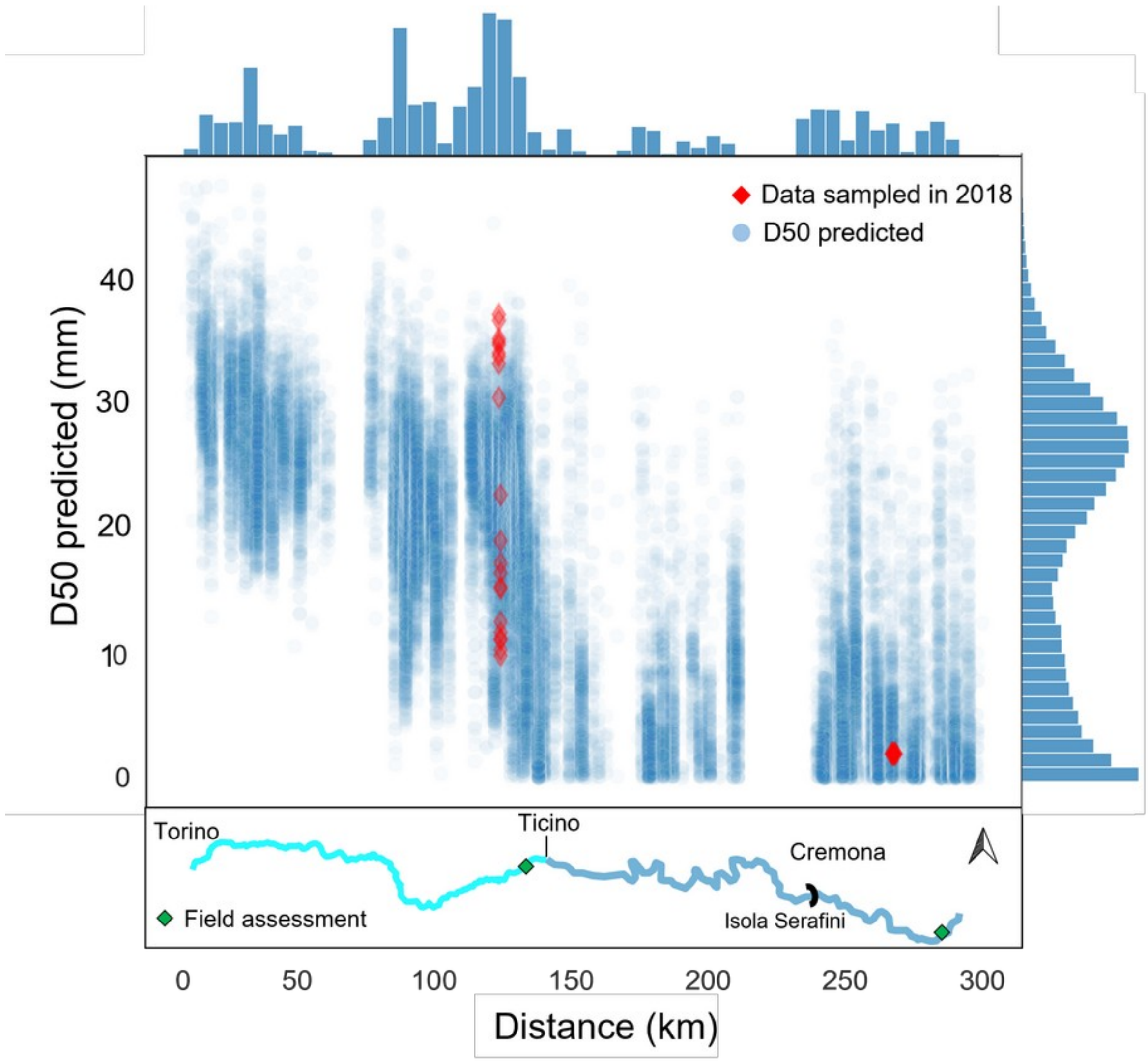
Data sampled in 2018
D50 predicted
D50 predicted (mm)
0
10
20
30
40
Torino
Ticino
Cremona
Isola Serafini
Field assessment
0
50
100
150
200
250
300
Distance (km)

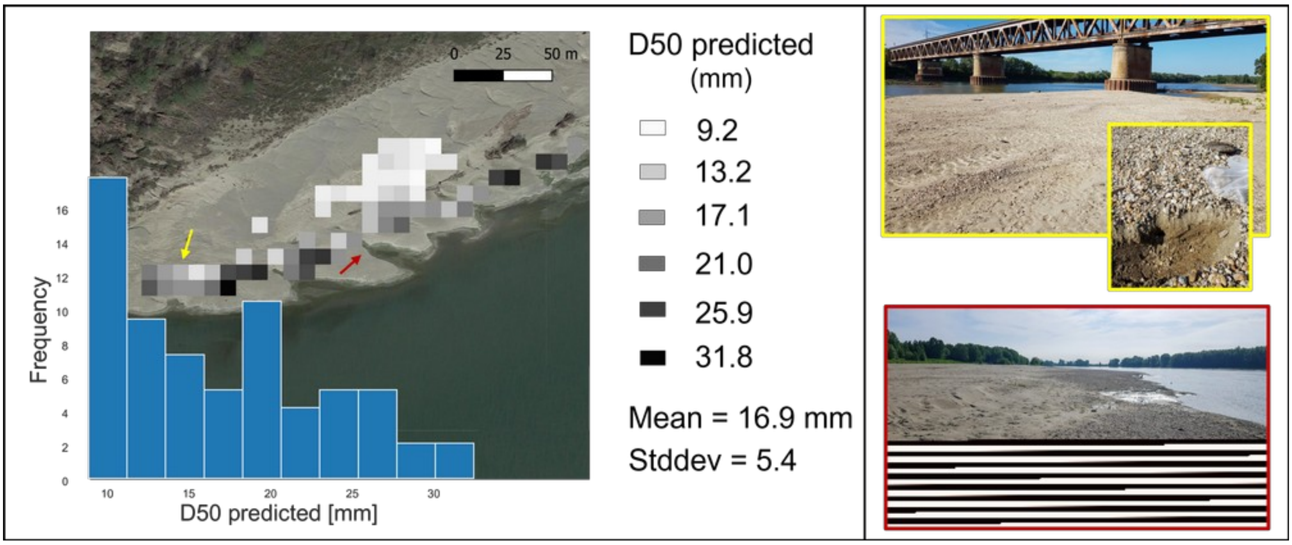

0 25 50 m
D50 predicted
(mm)
9.2
13.2
17.1
21.0
25.9
31.8
Mean = 16.9 mm
Stddev = 5.4
Frequency
0
2
4
6
8
10
12
14
16
10
15
20
25
30
D50 predicted [mm]

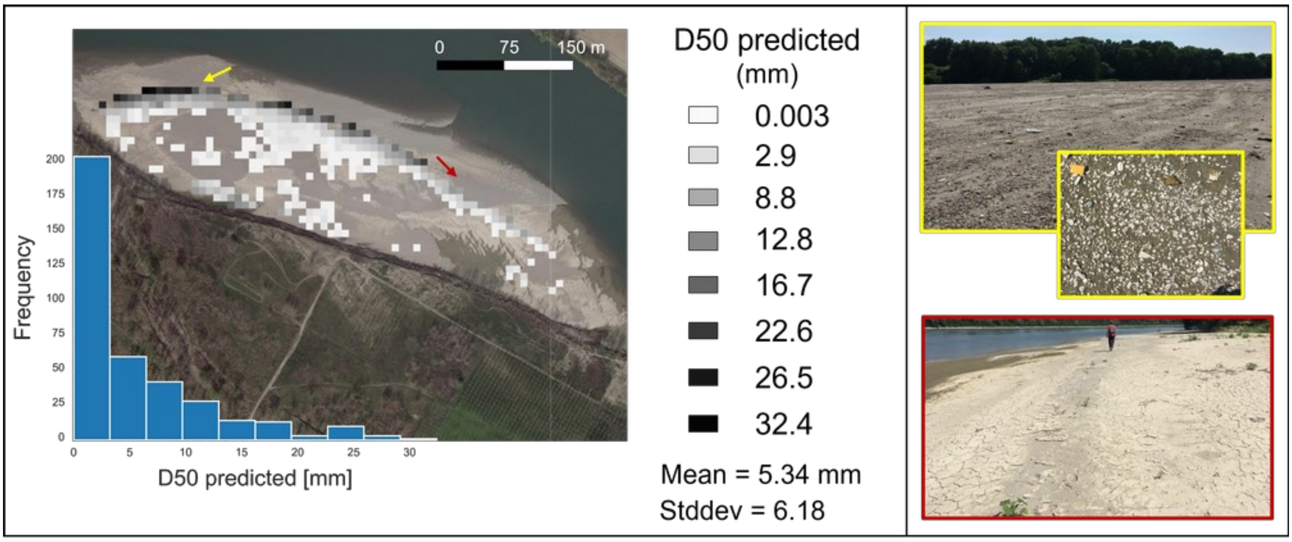

0
75
150 m
D50 predicted
(mm)
0.003
2.9
8.8
12.8
16.7
22.6
26.5
32.4
Mean = 5.34 mm
Stddev = 6.18
Frequency
200
175
150
125
100
75
50
25
0
0
5
10
15
20
25
30
D50 predicted [mm]